APL Photonics

Tutorial: Terahertz beamforming, from concepts to realizations

Cite as: APL Photonics **3**, 051101 (2018); https://doi.org/10.1063/1.5011063
Submitted: 29 October 2017 • Accepted: 02 January 2018 • Published Online: 06 February 2018

Daniel Headland, Yasuaki Monnai, Derek Abbott, et al.

Tutorial: Terahertz beamforming, from concepts to realizations

Daniel Headland,[1,2,a] Yasuaki Monnai,[3] Derek Abbott,[1] Christophe Fumeaux,[1] and Withawat Withayachumnankul[1,b]
[1]*School of Electrical and Electronic Engineering, The University of Adelaide, South Australia 5005, Australia*
[2]*Institute for High-Frequency and Communication Technology, University of Wuppertal, Wuppertal 42119, Germany*
[3]*Department of Applied Physics and Physico-Informatics, Keio University, Yokohama 223-8522, Japan*

(Received 29 October 2017; accepted 2 January 2018; published online 6 February 2018)

The terahertz range possesses significant untapped potential for applications including high-volume wireless communications, noninvasive medical imaging, sensing, and safe security screening. However, due to the unique characteristics and constraints of terahertz waves, the vast majority of these applications are entirely dependent upon the availability of beam control techniques. Thus, the development of advanced terahertz-range beam control techniques yields a range of useful and unparalleled applications. This article provides an overview and tutorial on terahertz beam control. The underlying principles of wavefront engineering include array antenna theory and diffraction optics, which are drawn from the neighboring microwave and optical regimes, respectively. As both principles are applicable across the electromagnetic spectrum, they are reconciled in this overview. This provides a useful foundation for investigations into beam control in the terahertz range, which lies between microwaves and infrared light. Thereafter, noteworthy experimental demonstrations of beam control in the terahertz range are discussed, and these include geometric optics, phased array devices, leaky-wave antennas, reflectarrays, and transmitarrays. These techniques are compared and contrasted for their suitability in applications of terahertz waves.
https://doi.org/10.1063/1.5011063

I. INTRODUCTION

The terahertz range is generally defined as the portion of the electromagnetic spectrum that lies between 100 GHz and 10 THz. It is situated above the microwave range, and below the optical regime, and hence the development of terahertz technologies draws upon techniques and knowledge from both domains. Thus, the terahertz range provides an opportunity to consolidate and reconcile the paradigms of microwave engineering with that of optics and photonics. That said, there exist challenges specific to terahertz technologies that deserve consideration here.

Whilst light and radio waves exist as phenomena on the same spectrum, they are separated by a technology gap.[1,2] On the lower end of the spectrum, electronic devices are generally employed to generate power, but such devices experience a low-pass response due to parasitic reactances. For the same reason, it is highly challenging to electronically amplify terahertz power. This limits output power of such devices at terahertz frequencies. Above the terahertz range, lasers are commonly employed, but gain media suitable for room-temperature lasing at terahertz frequencies are lacking, as electron energy-level transitions corresponding to photons of the appropriate wavelength become

[a]daniel.j.headland@gmail.com
[b]withawat@adelaide.edu.au

thermalized. Thus, despite close to a century of scientific interest,[3,4] the terahertz range remains under-utilized. That said, there is presently a significant amount of research interest into practical sources of terahertz power. Promising avenues for exploration include complimentary metal-oxide-semiconductor (CMOS) devices,[5,6] resonant tunneling diodes,[7,8] vacuum electronic sources,[9,10] and photonic devices.[11,12]

Another fundamental challenge facing terahertz frequencies is losses. For instance, terahertz waves experience strong absorption as they propagate in atmosphere,[13] which is partly due to the fact that key atmospheric molecules, particularly water, resonate in the terahertz range, and hence humid and rainy environments are particularly problematic. This issue can be largely mitigated by exploiting knowledge of atmospheric windows.[11] Additionally, metals are not ideal conductors in the terahertz range,[14] and dielectric materials that are amenable to fabrication at the appropriate scale, such as polymers, are often very lossy.[15–17] Thus, it can be challenging to produce efficient terahertz devices. In this way, absorption can prevent the terahertz-range adoption of techniques that are popular at lower frequencies.

On top of these challenges, the vast majority of terahertz-range devices and applications necessitate some form of beam control, which is loosely defined as the capacity to manipulate the shape and directionality of a given beam in some desirable way. For example, lenses and reflectors are fundamental components that channel the flow of terahertz waves along prescribed free-space paths, to localize their interaction with samples and detectors.[18] As such, the development of terahertz spectroscopy applications is contingent upon the availability of beam-control devices. These applications include pharmaceutical quality control[19,20] and the detection of hazardous and controlled substances,[21] as several molecules of interest such as those possessed by drugs[22,23] and explosives[24,25] exhibit discernible spectral features in the terahertz range. Additionally, spectroscopic investigations into chiral molecules can be aided by advanced beam-control devices that separate left- and right-handed circular polarization into different outgoing-beam directions, so as to probe their response separately.[26] This is useful because many molecules in biology and chemistry are chiral and respond differently to left- and right-hand circularly polarized terahertz waves.[27–29]

Terahertz-range imaging applications[30] such as safe, subdermal medical imaging,[31–33] security screening,[34] and non-destructive imaging of priceless artifacts and art[35,36] are envisaged, as terahertz waves are non-ionising, and can penetrate to a modest depth in soft tissues[37] and clothing.[38] Such non-contact imaging applications typically rely on some form of beam control—either fine beam-focusing[30,39] or Bessel beams,[40] to provide adequate resolution. If combined with a mechanically scanned detector array, beam-focusing can be integral to terahertz-range light-field imaging systems, which provide directional information about incoming rays, and make it possible to re-focus an image post-capture.[41] Lastly, dynamic beam scanning capabilities could potentially enable short-range terahertz radar,[42] where the short wavelength makes it possible to register fine details. This has potential for sensing applications including collision-avoidance and flight support for small autonomous aircraft and human gesture recognition in wearable devices. Such applications can be achieved with frequency-scanning, which is offered by relatively simple leaky-wave antennas[43] and flat beam deflectors.[44]

Terahertz frequencies are promising for communications applications due to the large quantity of absolute spectral bandwidth available and the correspondence between spectral bandwidth and achievable data rate.[45,46] For this reason, terahertz communications links can provide data rates of several tens of Gbps, and this has been confirmed by numerous practical experiments.[11,47–53] However, due to the increasing free-space path loss at terahertz frequencies and above, terahertz links must waste as little power as possible in order to achieve adequate signal power over a useful propagation distance. For this reason, terahertz communications must minimize the amount of power that is projected into the directions in which it will not be received. Thus, highly directive beamforming is required, and this necessitates devices with large physical aperture. As the aperture of most terahertz sources is limited, a large aperture is typically achieved by means of lenses[52,53] or reflector dishes.[11] Flat-profile devices such as reflectarrays and transmitarrays present a compact alternative to such devices.[54] Although the latter options require greater complexity and are of lower bandwidth, reflectarrays[55,56] and transmitarrays[57] can exhibit birefringence for polarization-dependent multiplexing. This can be used to effectively double the capacity of a single beam, as distinct messages can be encoded into

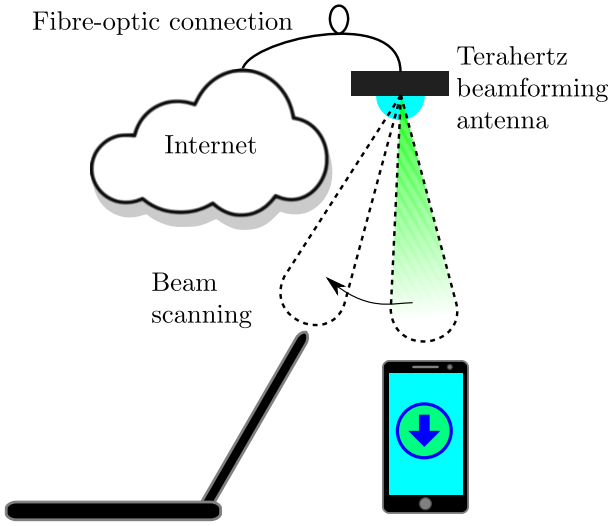

FIG. 1. Illustration of a future terahertz-range indoor communications system, which employs beam control techniques to achieve high directivity, maintain alignment, and to switch between different devices.

both polarizations. Additionally, reflectarrays and transmitarrays have greater potential for dynamic beamforming,[58,59] in a manner similar to phased-array antennas. Dynamic scanning of this sort is a highly desirable goal, as it has the potential to support automatic alignment in future terahertz links. Additionally, beam-scanning capabilities would allow a directional terahertz beam to switch between multiple devices rapidly, as illustrated in Fig. 1, for on-demand high-volume connections.

This article presents an overview of previous efforts in the field of terahertz beam control across a broad range of applications. In order to provide some conceptual grounding to this work, the theoretical basis that underpins all discussed beam control techniques is presented briefly in Secs. II–IV. The presentation of this information reconciles theories developed and used independently in the microwave and optical ranges. As such, the information that is given in these sections is not particular to the terahertz range, but rather, it applies to the entire electromagnetic spectrum up to the point at which quantum effects dominate, and a classical Maxwell's paradigm is no longer strictly valid. Thereafter, specific beamforming techniques, with noteworthy terahertz-range demonstrations reported in the literature, are given in Secs. V–VIII. Finally, these efforts are compared and contrasted in Sec. IX. It is noted that we adopt the engineering phase convention in this tutorial, under which the propagation of a wave through distance d in free space can be expressed mathematically as multiplication by the term $\exp(-jk_0d)$, where k_0 is the free-space wavenumber. As such, the phase that is acquired as the wave propagates is a negative number.

II. MODELS FOR WAVE PROPAGATION

The models for wave propagation that are presented in this section have been founded upon Maxwell's equations, which are a strictly wave-oriented paradigm. Section II A concerns the relationship between the field distribution over a given diffracting aperture and the field pattern of the ensuing propagating beam. On the other hand, Sec. II B involves the relationship between the pattern of excitation on an array antenna and a radiation pattern in the far field. Both scenarios depend upon the principle of linear superposition of electromagnetic waves, which states that, in the presence of a number of sources, the field at a given point in space is the complex vector sum of the fields that are output by these individual sources. It is also noted that the contribution made by a given source depends upon the distance from the source to the relevant point in space, as waves acquire phase progressively as they propagate, and the amplitude decreases with distance due to path loss. This principle of linear superposition is illustrated in Fig. 2. Lastly, although electromagnetic waves are vector quantities, they are treated as complex-valued scalars in order to simplify the following

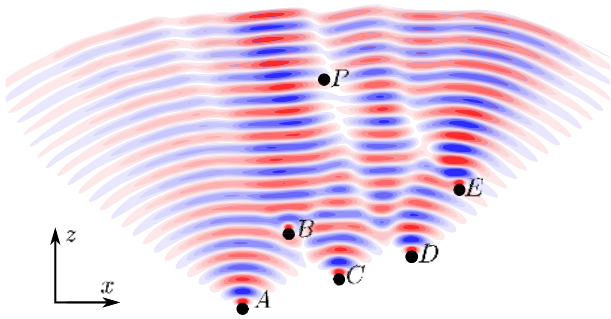

FIG. 2. Electromagnetic waves obey the law of linear superposition, whereby the field at a given point (P) can be expressed as the sum of the fields emanating from any number of sources (in this case, A–E). This field is subject to the radiation pattern of each source, which describes angular dependence of projected power. Additionally, as the field propagates from the source to point P, it experiences a phase change due to distance and free-space path loss due to the field's spreading over a larger surface area. It is noted that any effects due to sources physically blocking the fields from other sources, or reactive coupling between adjacent sources, are neglected in this diagram.

discussion, and hence polarization has been neglected. This is a common approach in an optics context.

A. Huygens' principle

Christiaan Huygens posited in 1678 that a given wavefront can be considered analogous to an array of infinitesimal secondary sources, which are now known as "Huygens' point sources" or "Huygens' source radiators."[60,61] Each source was thought to produce a spherical wavelet in Huygens' initial work, but it is noted that this would produce a backward-propagating wave, and this is not observed in practice. In the current understanding, each Huygens' source can be considered an orthogonal pair of infinitesimal electric and magnetic dipoles, which radiate in a broad angle that is centered upon the direction defined by their cross-product. The wavefront at a later instant can therefore be found by constructing the "envelope" of the secondary wavelets, which can be considered the overall, shared boundary formed by all wavelets collectively. The subsequent wavefront similarly generates the wavefront that follows, and so on, as the wave propagates through space. Augustin-Jean Fresnel later expanded upon the insight provided by Huygens, and by allowing the secondary sources to interfere, was able to mathematically formulate Huygens' principle. The result of his investigation is now known as the Huygens-Fresnel diffraction integral, but it is noted that this result was found empirically, as with Huygens' principle, and hence was not derived from a more fundamental theory. Finally, Gustav Kirchhoff was able to ground this theory in a sound mathematical footing. By employing a scalar form of the differential wave equation, Kirchhoff showed that the Huygens-Fresnel principle is an approximation of results that are derivable from fundamental principles.

It is noted that methods are available that can provide a greater degree of accuracy than the scalar form of Huygens' principle. For instance, a vectorial treatment of Huygens' principle is offered by Schelkunoff's surface equivalence theorem.[62] This rigorous treatment includes both electric and magnetic equivalent vector sources, and both near- and far-fields can be computed by the vector potential formalism. This approach is preferred in the microwave range, as it fully describes polarization effects and maintains a complete description of the near fields. However, the formulation of scalar diffraction theory is more straightforward and is of sufficient accuracy provided that the diffracting aperture is larger than a wavelength and that diffracting fields are observed at a sufficient distance from the aperture.[63]

The Huygens-Fresnel model approximates electromagnetic radiation as a scalar and predicts diffractive behaviors that are not covered by a straightforward ray-tracing paradigm. Thus, it is often referred to as "scalar diffraction theory." Using this principle, one may evaluate the complex amplitude of the electromagnetic wave at an arbitrary point, $A(x, y, z)$, from a given complex field distribution at an aperture, $A(\xi, \eta, 0)$, as follows:[61]

$$A(x,y,z) = \frac{1}{j\lambda}\iint_{\Sigma} A(\xi,\eta,0)\,\frac{\exp(-jkr_{01})(1+\cos\psi)}{2r_{01}}\mathrm{d}\xi\mathrm{d}\eta, \tag{1}$$

where ξ and η substitute for the x and y components on the aperture, respectively, and $A = a\exp(j\varphi)$ is the complex field amplitude, for which a and φ represent the magnitude and phase components, respectively. For this analysis, the aperture is orthogonal to the z-axis and is situated at $z = 0$. The distance from $(\xi,\eta,0)$ to (x,y,z) is $r_{01} = \sqrt{(x-\xi)^2 + (y-\eta)^2 + z^2}$, ψ is the angle that a line connecting these two points makes with the z-axis, and k is the wavenumber in the relevant medium. Equation (1) is a valid approximation, provided that $r_{01} \gg \lambda$, which is not difficult to observe in practical cases. The $(1+\cos\psi)/2$ term in Eq. (1) is known as the "obliquity factor," and it defines the angular spread of the radiation, or radiation pattern, that is projected by an individual infinitesimal crossed-dipole Huygens' source. Also, it is noted that this integral is generally calculated as a Riemann sum, which facilitates the analysis of arbitrary field distributions for the diffracting aperture.

If the distance, z, is significantly greater than the aperture size, then $(1+\cos\psi)/2 \approx 1$ and $z \gg x, y \gg \xi, \eta$ in Eq. (1), and it can be approximated with the following form:[60]

$$A(x,y,z) = \frac{\exp(-jkz)}{jz\lambda}\iint_{\Sigma} A(\xi,\eta,0)\,\exp\left(jk\left[\frac{x\xi}{z} + \frac{y\eta}{z}\right]\right)\mathrm{d}\xi\mathrm{d}\eta. \tag{2}$$

It is noted that this integral is a form of the two-dimensional Fourier transform, with spatial-frequency components $x/(z\lambda)$ and $y/(z\lambda)$. Thus, the beam pattern projected by a given aperture ultimately converges to the spatial-frequency transform, and hence this mapping can provide insight into the relationship between aperture distribution and field pattern at a sufficient distance. This approximation of the Huygens-Fresnel principle is known as the Fraunhofer diffraction.

B. Array theory

Conceptually, the Huygens-Fresnel principle is directly analogous to the notion of "array factor," which is a useful approach to understand the behavior of array antennas. Both seek to express overall radiated field as a linear superposition of fields from smaller sources. The difference is that, in the case of the Huygens-Fresnel principle, these sources are virtual and infinitesimal, whereas in the case of array theory the sources are the actual and finitely sized antenna elements that make up the array. Another difference is that the Huygens-Fresnel principle seeks to determine field projected to a point in the Cartesian space, a finite distance away from the radiating aperture, whereas array theory aims to determine the electric field projected into a given direction in spherical coordinates, in the far field. This coordinate system is characterized by the angle that a given direction makes with the z-axis, θ, and the angle that the projection of this direction upon the xy-plane makes with the x-axis, ϕ.

A general expression for the array factor of a rectangular planar array that contains $M \times N$ elements, with spacing d_x and d_y, is given[64] in the following equation:

$$\mathrm{AF}(\theta,\phi) = \sum_{m=1}^{M}\sum_{n=1}^{N} A_{mn}\exp(jk[md_x\sin\theta\cos\phi + nd_y\sin\theta\sin\phi]), \tag{3}$$

where the mnth element has complex amplitude $A_{mn} = a_{mn}\exp(j\varphi_{mn})$. It is noted that Eq. (3), when expressed in Cartesian coordinates, can be considered equivalent to Eq. (2), under the conditions that $z \to \infty$ and that θ is small. For an array of identical radiators, Eq. (3) is multiplied by the radiation pattern of the individual element in order to derive the overall radiation pattern. However, it is often desirable to know the array factor in isolation, especially when the beam-shaping properties of the array are of greatest interest.

Due to differences in physical scale, and the requirements of different applications, an array-theory approach is generally most relevant at radio and microwave frequencies. However, at higher frequencies, a beam-oriented paradigm is most relevant, and hence techniques such as the Huygens-Fresnel principle are preferred for optics. For terahertz frequencies, the choice of paradigm is informed by application. However, at a more fundamental level, both paradigms are equally valid across the electromagnetic spectrum, as the phenomena that they describe are equivalent.

III. BEAMFORMING

Section II shows that the propagating behavior of a given beam can be wholly determined by its original field distribution over a transverse plane, provided the beam propagates in a linear, uniform, and isotropic medium. Thus, specific desired propagating beam behaviors can be prescribed by informed manipulation of this field distribution, and in particular, the phase distribution. This correspondence between field distribution at the aperture and the subsequent behavior of the propagating beam is the essence of what is known as "wavefront engineering" or "beamforming." For simplicity, field distributions will be considered abstractly in this section, without providing an explanation of how a given field distribution is synthesized. Likewise, specific frequencies of operation will not be given, and when the wavelength is invoked, it is simply a variable. This is to better communicate the core concepts of wavefront engineering, without the added complexities of implementation.

Four representative beam-shaping operations are presented in this way, namely, the generation of a plane wave, beam deflection, Bessel-beam generation, and beam focusing. These are chosen as they are generic and cover the vast majority of beam control demonstrations to be presented in Secs. V–VIII. Lastly, these beam control techniques are presented in terms of an outgoing wave, i.e., the phase distribution in question is that of a transmitting aperture. This is chosen for simplicity, but it is noted that the principle of reciprocity dictates that the propagation direction can be reversed without disturbing the overall beam pattern. Thus, these beam control techniques can, in principle, be utilized for transmitters and receivers alike. In practical cases, however, certain phasing techniques are inseparable from the wave generation mechanism and are thus only available to radiated beams. On the other hand, receivers have more choice with regards to virtual beamforming techniques, which is essentially the use of synthetic aperture distributions in postprocessing.[65] However, discussions on signal processing techniques of this sort are beyond the scope of this article.

A. Uniform phase

The simplest possible case of a phase distribution is entirely uniform. The behavior of the subsequent propagating beam can be understood in terms of Huygens' principle. In this instance, all infinitesimal secondary sources (as per Huygens' paradigm) are in-phase, and hence the envelope that is constructed from their fields is approximately planar and parallel to the previous wavefront upon which the aforementioned auxiliary sources are situated, as illustrated in Fig. 3(a). There will, however, be some degree of convexity to the outgoing wavefront, which produces beam divergence, due to the finitely sized aperture. The effects of aperture size will be discussed in Sec. IV A. A uniform phase distribution in the xy-plane is illustrated in Fig. 3(e), and the ensuing beam behavior, employing Gaussian-beam excitation, is shown as a propagating beam profile in Fig. 3(i). It can be seen that a single beam is produced, which travels in the positive-z direction. This is supported by the far-field radiation pattern given in Fig. 3(m), which is constructed using array theory. Thus, a uniform phase distribution is useful for applications in which the radiated beam is intended to travel in one specific direction, such as a point-to-point communications link or a radio telescope. As the change in wavefront shape is minimal, this beam is capable of transmitting energy over great distances, with little angular divergence as described by the paraxial Gaussian beam approximation. However, it is noted that this low divergence holds true only when the aperture size is much larger than the wavelength.

B. Beam deflection

If an aperture is viewed from an oblique angle, then one side of the aperture is further away from the observer than the other. As a consequence, the waves emanating from the far side will acquire more (negative) phase than the near side as they propagate from the aperture to the observer. To project energy toward the observer, a linear phase ramp at the aperture is thus required to negate the negative phase accumulation on the far side. Thus, directionality of an outgoing beam is dictated by the slope of an applied phase ramp, as illustrated in Fig. 3(b). This is known as "beam deflection" or "beam steering," and the required phase distribution, φ, for steering toward an angle $+\theta_s$ from the

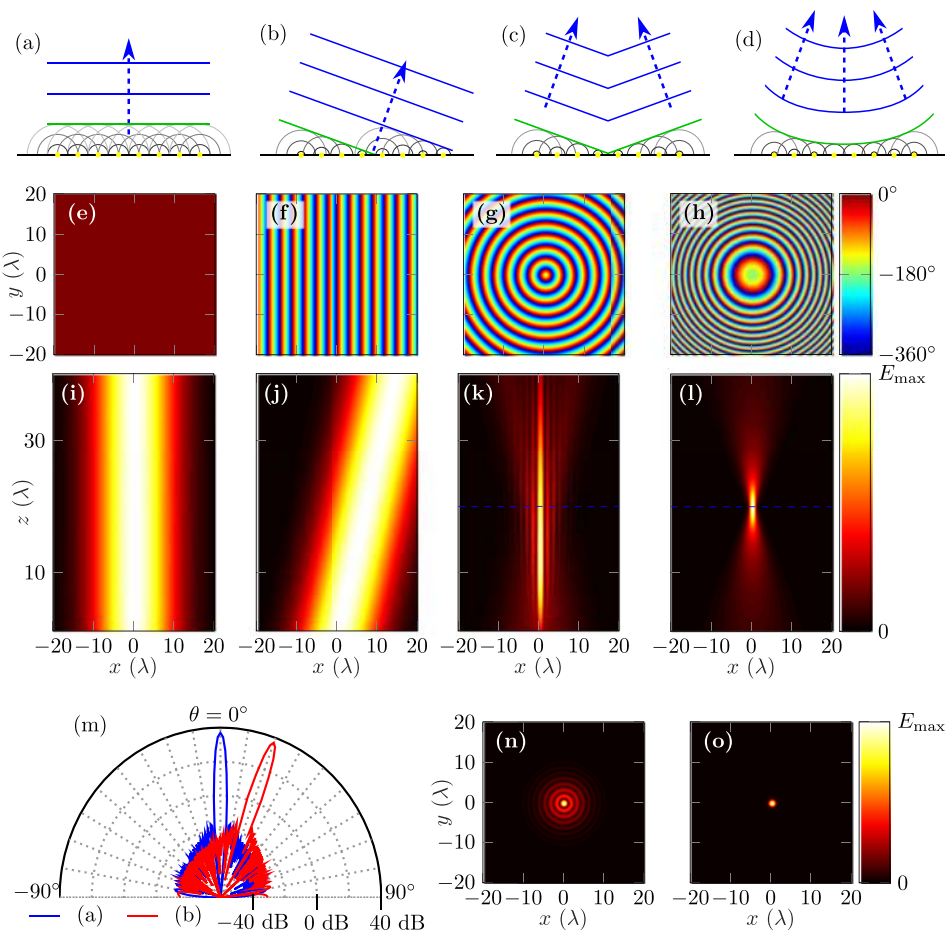

FIG. 3. Illustration of the correspondence between phase control and beam control, showing [(a)–(d)] Huygens'-principle diagrams of plane wave propagation, beam deflection, Bessel beam formation, and focusing, respectively. Examples of phase distributions that produce each of these beam shapes are shown in [(e)–(h)], and the corresponding propagating beams are shown below in [(i)–(l)]. The far-field radiation patterns produced by (e) and (f) are shown in (m), and cross sections of the beams produced by (g) and (h) are shown in (n) and (o), respectively, where their intersections with (k) and (l) are shown with dashed blue lines. Plots (i)–(o) are generated numerically with Eq. (1), with the exception of (m), which is generated with Eq. (3). For these calculations, a 2D Gaussian function of $1/e$-width 20λ is employed as the magnitude distribution of the radiating aperture, to mitigate edge effects. To facilitate Riemann-sum calculation, field distributions are discretized in steps of $\lambda/4$. All field magnitude plots are in linear scale and normalized to their own respective maxima.

z-axis in the xz-plane is as follows:

$$\varphi(x) = -k_0 x \sin\theta_s, \tag{4}$$

where k_0 is the free-space wavenumber. This ensures that waves traveling in the direction θ_s will be in phase, and hence constructive interference will be experienced in this direction by the fields that are output by the auxiliary sources of Huygens' principle. It is noted that, as 0° is equal to −360°, the linear phase ramp is wrapped to a sawtooth function that is limited to a single phase cycle. A sawtooth function of this sort is periodic, with spatial periodicity D. As such, its functionality can be considered equivalent to that of a diffraction grating. The grating equation, which governs the output directionality of such devices, is as follows:

$$D\sin\theta_s = m\lambda, \quad m = 0, \pm 1, \pm 2, \ldots, \tag{5}$$

where m denotes the diffraction order. In the case of the aforementioned sawtooth phase distribution, the $m = +1$ diffraction order corresponds to Eq. (4) exactly, where $\varphi = -2\pi$ and $x = D$. A sawtooth phase distribution, for deflection out to a +20° angle, is illustrated in Fig. 3(f). The corresponding

propagating beam profile is given in Fig. 3(j), and the associated far-field radiation pattern is given in Fig. 3(m). Both show that the directionality of the output beam is as intended and that the behavior of the beam is equivalent to the previous uniform-phase example.

Beam deflection functionality provides the general utility of control over a beam's directionality. If the slope of the phase ramp is dynamically adjustable, then either beam scanning or switched-beam functionality is achieved. In the former case, this means that the directionality of a beam can be continuously swept through a given range of angles, and in the latter, there are finitely many outgoing beam directions to choose from. This is highly useful to distinguish between different directions in the far-field, and hence it finds extensive use in applications such as radar, including collision-avoidance radar for automotive safety applications.[66] Such functionality also facilitates automatic alignment of point-to-point communications links, as in the illustration given in Fig. 1.

C. Bessel beam

The previous two examples have concerned beam behaviors that are most useful in the far-field. However, different phase distributions can be employed to produce beams with features that are of greatest interest at a shorter distance from the radiating aperture. If, for example, the phase distribution given in Eq. (4) is made radially symmetric about the optical axis (i.e., z-axis), then the following phase distribution results:

$$\varphi(x, y) = k_0 \left(\sqrt{x^2 + y^2} \right) \sin \theta_s. \tag{6}$$

In principle, this is closely related to beam deflection, with the important difference that all fields are directed toward the optical axis, as illustrated in Fig. 3(c). The interference of these fields leads to an overall beam shape that is quite different to the aforementioned beam deflection example. An example phase distribution is given in Fig. 3(g), which makes use of a deflection angle of 20°, as in the previously discussed beam-deflection example. The resulting field profile in the xz-plane is given in Fig. 3(k), and the cross section in the xy-plane, at a distance of 20λ from the radiating aperture is given in Fig. 3(n). This is known as a Bessel beam.[67,68] A long column of constructive interference can be seen along the optical axis, and this is the main useful component of this beam pattern. There are also surrounding fringing fields that form a series of concentric rings. For a given xy-plane cross section, these concentric rings are an interference pattern, which is produced by the superposition of the wave that has already passed through the optical axis at an earlier instant with the wave that will pass through the optical axis at a later instant. Such a beam can be employed for applications including the detection of objects within the vicinity of the Bessel beam's range.[69] Additionally, the long, narrow line of high-intensity radiation makes Bessel beams well suited to certain forms of imaging, which have been demonstrated across the electromagnetic spectrum.[70,71]

D. Focusing

In the previous example, a radially symmetric, linear-ramp field distribution is employed to produce the convergence of an outgoing beam along the optical axis. If, however, a paraboloid curve is utilized rather than a linear ramp, as illustrated in Fig. 3(d), it is possible to produce a single focal point on the optical axis. In order to achieve convergence upon a point on the z-axis at a distance F away from the radiating aperture, the following phase distribution can be employed:

$$\varphi(x, y) = k_0 \left(\sqrt{F^2 + (x^2 + y^2)} - F \right). \tag{7}$$

For each Huygens' source on the diffracting aperture, this phase distribution will essentially compensate the particular negative phase that a wave acquires whilst traveling from the position of that auxiliary source to the focal point. Thus, the phase of the waves output by all auxiliary sources is identical at the focal point, thereby producing constructive interference. An example of such a phase distribution, with a focal length of 20λ, is illustrated in Fig. 3(h), and the resulting propagating beam profile and cross section are shown in Figs. 3(l) and 3(o), respectively. It is clearly shown that the radiation from the aperture converges to a fine point. Such localization of electromagnetic waves

is extremely useful for a diverse range of applications, where it can be used to isolate matter-field interaction to a specific small volume.

E. Other beam shapes

The four beam control techniques given in Secs. III A–III D are certainly important examples due to the wide range of applications that make use of them. However, it is noted that this is not an exhaustive list; there is no limit to the number of different phase distributions available, and each will have some associated beam behavior. More sophisticated examples include a spiral phase distribution, which gives rise to a beam that possesses orbital angular momentum[72] and so-called "bottle beams," which have a dark "anti-focus" that is surrounded in all directions by regions of higher intensity.[73]

Greater freedom is provided by techniques such as the Gerchberg-Saxton phase retrieval algorithm,[74] which make it possible to prescribe a near-arbitrary field magnitude distribution in the Cartesian space and iteratively calculate a phase distribution that will produce the bespoke field distribution. Additionally, shaped-beam techniques are available in the far-field, which provide highly customizable radiation patterns.[75,76]

IV. PRACTICAL CONSIDERATIONS

A. Effects of aperture size

In this context, the aperture can be loosely defined as the hypothetical area that a radiator or receiver can utilize for the emission or interception of electromagnetic waves. In practical cases, this is closely related to the physical area of a device, but a device will rarely make use of its entire area in a perfect manner, and hence the effective aperture is generally smaller than physical size.

The aperture is of crucial importance to beam control techniques. For instance, the outgoing wavefront is not strictly planar in the plane wave-based example given in Sec. III A, in spite of the uniform phase distribution. This is because the aperture is finite, and hence Huygens' principle dictates that the auxiliary sources at the edge of the aperture cause the overall envelope to curve outward at the edges. This is known as diffraction, and it gives the outgoing wavefront a degree of convexity, which is the origin of beam divergence in uniform-phase apertures. For this reason, there is some finite angular spread in the radiation patterns shown in Fig. 3(m). If, on the other hand, the aperture were of infinite extent, then there would be no divergence of this sort, and hence the radiation pattern would take the form of a Dirac delta function in the direction of the main lobe. This correspondence is consistent with Eq. (2), as it is well known that a function of broad extent typically has a narrow Fourier transform. As an illustration, beam profiles resulting from a uniform phase distribution, with progressively smaller aperture, are illustrated in Figs. 4(a), 4(e), and 4(i) and likewise with a linear ramp phase distribution in Figs. 4(b), 4(f), and 4(j). In both cases, it can be seen that the divergence of the beam increases as aperture decreases, as expected.

An antenna's beam divergence is quantified with the notion of antenna gain, G, which is defined for a transmitting antenna as the ratio of radiation intensity that is projected into the desired direction to the radiation intensity that would be achieved with a hypothetical, perfectly efficient and isotropic radiator. In general, an aperture of larger electrical size produces higher antenna gain. In the context of a point-to-point communications link, the antenna gain can be employed in the Friis transmission equation[77] to determine the ratio of power transmitted to power received, over propagation distance L,

$$\frac{P_{\text{Received}}}{P_{\text{Transmitted}}} = G_{\text{Transmitter}} G_{\text{Receiver}} \left(\frac{\lambda}{4\pi L}\right)^2. \tag{8}$$

In this scenario, there is a deficit in P_{Received} that is not due to absorption in the transmission medium or the non-ideal efficiency of either antenna. Rather, it is because that not all transmitted power is successfully intercepted by the receiver. This is known as free-space path loss. It can be seen from Eq. (8) that free-space path loss is proportionate to the square of frequency, which places terahertz

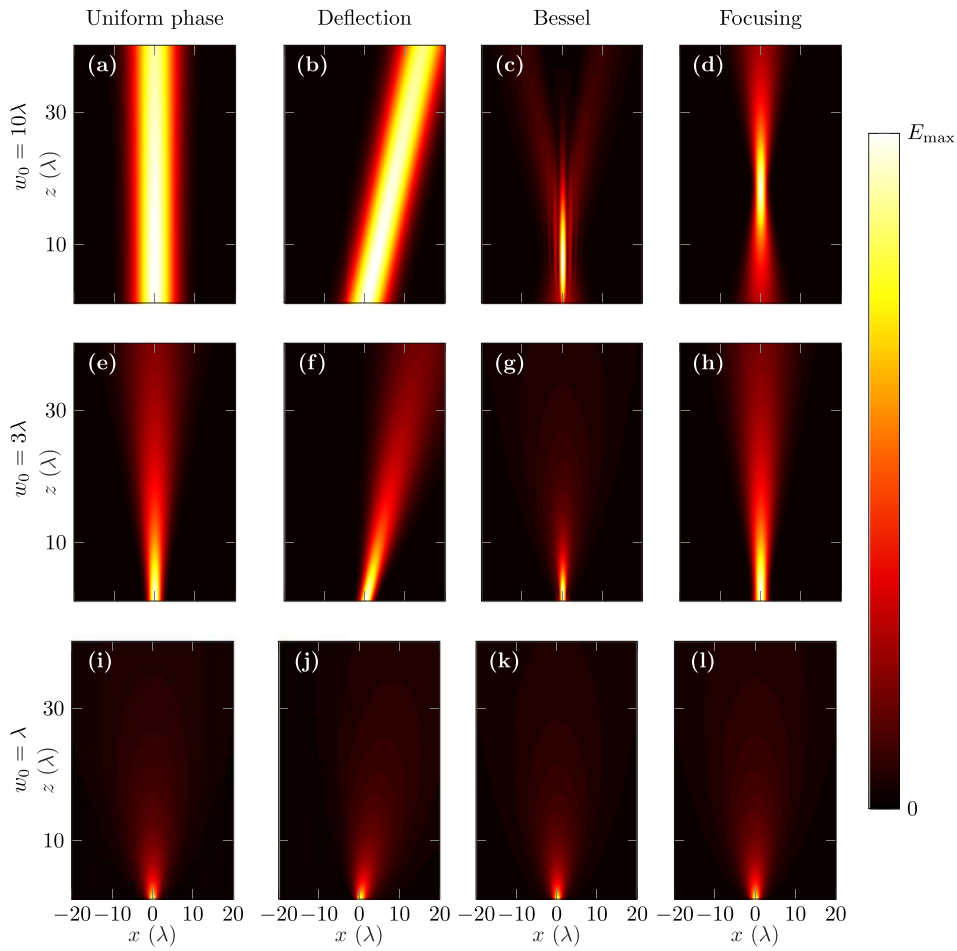

FIG. 4. Illustration of the relationship between aperture and beam control. A 2D Gaussian function of 1/*e*-width $w_0 = 10\lambda$ is employed as a field magnitude distribution, which is coupled with the phase distributions in Figs. 3(e)–3(h) to generate the propagating field plots in [(a)–(d)], by means of Eq. (1). Gaussian functions of 1/*e*-width $w_0 = 3\lambda$ and $w_0 = 1\lambda$ are employed to generate [(e)–(h)] and [(i)–(l)], respectively. All plots are in linear scale and normalized to their own respective maxima.

radiation at a disadvantage in comparison to the lower frequencies that are more usually employed for free-space communications. This exacerbates the power-related constraints discussed in Sec. I. For this reason, it is crucial that terahertz communications links make use of electrically large aperture for both the transmitter and receiver, so as to have large values of $G_{\text{Transmitter}}$ and G_{Receiver} to counteract the path loss.

For a Bessel beam, the illumination along the optical axis is dependent upon the existence of fringing fields that are converging upon this axis. The fringing fields that pass through the optical axis at the furthest point in the Bessel beam's range are those emitted from the edge of the aperture. Thus, the aperture size dictates the length of illumination along the optical axis for a Bessel beam. In the hypothetical case of infinite aperture, and hence infinite energy, this length will likewise be infinite. By contrast, as illustrated in Figs. 4(c), 4(g), and 4(k), progressive shrinking of aperture results in a corresponding reduction in the length of the optical axis that is illuminated in this way.

For a focused beam, the aperture size has a close, inverse relationship with the width of the focal spot. A larger aperture will, in general, produce a finer, more concentrated focal spot. This relationship is illustrated in the discrepancy between Figs. 3(l) and 4(d), where the Gaussian beam width is 20λ and 10λ, respectively. However, the focal spot size cannot be shrunk down to a singularity, as with the angular spread of the aforementioned plane-wave example, due to the diffraction limit,[78] which places a lowerbound at the order of a half-wavelength. Interestingly, in Figs. 4(h) and 4(l), there

is no apparent focal spot. Evidently, the inward wavefront curvature due to the phase distribution is overpowered by the outward wavefront curvature of diffraction due to finite aperture in these cases.

Lastly, the similarity of the small-aperture beams given in Figs. 4(i)–4(l) is noted. This is because smaller apertures approach a single point-source, for which no phase distribution can be prescribed. As such, control over a phase distribution is not sufficient for beam control. Rather, the lateral extent that is covered by this phase distribution is crucial to ensure an adequate degree of control over the resulting beam shape. Furthermore, Eq. (2) provides some insight into the large divergence of these beams, as a narrow aperture distribution function will have a broad-spread Fourier transform.

B. Effects of phase quantization

Up to this point, it has been taken for granted that a full, continuous phase cycle is always achievable. In practical cases, however, quite often only a finite number of phase levels can be implemented. That is to say, a 360° cycle is divided evenly into a certain, finite number of steps. Thus, a quantized phase distribution is essentially an approximation of the continuous-valued function. A consequence of this is that the outgoing beam is likewise an approximation of the intended beam shape, and hence some aberration is produced. At times, the use of phase quantization of this sort can be a response to the absence of a full 360° tuning range. For instance, if only a 300° tuning range is available, one may divide a 360° cycle into six steps of 60° each. Thus, the next step beyond 300° is 360°, which is equivalent to 0°.

The impact of phase quantization on overall performance is considered. To this end, the phase distributions given in Figs. 3(f)–3(h) are quantized to different degrees, and the ensuing beam behavior is illustrated in Fig. 5. It is noted that the uniform phase distribution given in Fig. 3(e) is not considered for this purpose. In terms of beam shape, Figs. 5(a)–5(f) show that the impact of eight and even four quantization levels is not especially severe. Some aberration is evident in both the beam deflector and the focusing example, but the desired functionality is still clearly represented. Interestingly, the Bessel beam shapes in Figs. 5(b) and 5(e) are not visually distinguishable from their continuous-valued counterpart in Fig. 4(c), which is an indication that Bessel beams are not affected especially strongly by phase quantization.

The impact of beam shape is most evident for the case of two quantization levels, 0° and 180°, which is also known as binary phase. In the case of a binary-phased deflector, the orientation of the slope that gives rise to deflection is ambiguous, and it converges to the pattern of a diffraction grating. Thus, a binary-phased deflector will exhibit a symmetrical beam pattern, which is clearly visible in Fig. 5(g). For the binary-phased Bessel beam, this bidirectional deflection is evidenced in weak rays that are directed away from the optical axis and do not contribute to the desired field pattern. The binary-phased focusing exhibits a similar pattern of weak rays, as well as a number of un-desired sub-foci between the radiating aperture and the main focus. Note that a binary-phased focusing device is commonly known as a zone plate.

The efficiency penalty of quantization can be quantified with the notion of diffraction efficiency, which is defined as the fraction of incident optical power that appears in a single diffraction order.[61] In this case, this diffraction order corresponds to the desired beam-shaping functionality, and other orders are essentially radiation projected into undesired directions. Thus, it is possible to calculate the diffraction efficiency by determining the field intensity that is projected into specific desired direction or position and then comparing it to the un-quantized case. The results of this comparison are presented in Fig. 6. It can be seen that diffraction efficiency increases with the number of achievable phase levels, as expected. For binary phase, diffraction efficiency is consistently below 50%. This is to be expected due to the aforementioned ambiguity of the phase distribution's slope; in general, half of the available power is projected elsewhere. From the results of larger numbers of quantization levels, however, it is evident that relatively few phase levels are required for a reasonable degree of efficiency. It is noted that these values of diffraction efficiency will not necessarily generalize, as the impact of quantization will vary with specific choice of aperture and phase distribution. Thus, it is only intended as a guide.

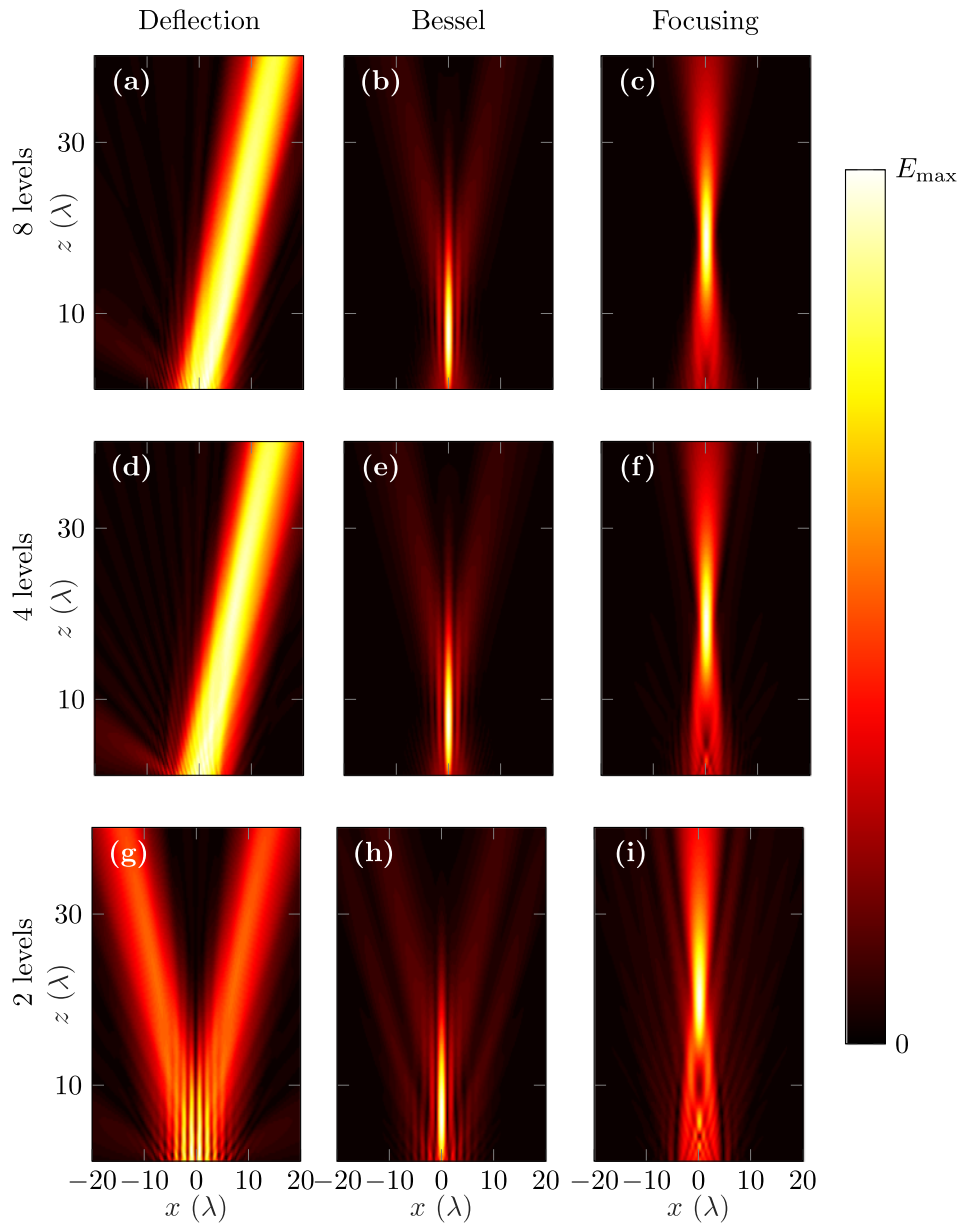

FIG. 5. Illustration of the impact of phase quantization upon beam control. The phase distributions in Figs. 3(f)–3(h) are quantized into eight levels to produce the beam profiles given in [(a)–(c)], four levels for [(d)–(f)], and two levels for [(g)–(i)]. A 2D Gaussian function of $1/e$-width 10λ is employed as a field magnitude distribution in all cases. All plots are in linear scale and normalized to their own respective maxima.

V. PATH-LENGTH OPTICS

As a wave travels through a dielectric medium, it acquires a phase delay that is proportional to the distance traveled, l, the refractive index of the relevant medium, n, and the frequency of that wave,

$$\varphi_{\mathrm{PL}}(l) = -k_0 n l, \tag{9}$$

where k_0 is the free-space wavenumber. Thus, phase can be manipulated by controlling either the distance that a wave travels or the refractive index of the relevant medium or both. For instance, a wave passing through a dielectric (i.e., $n > 1$) slab experiences a delay relative to propagation

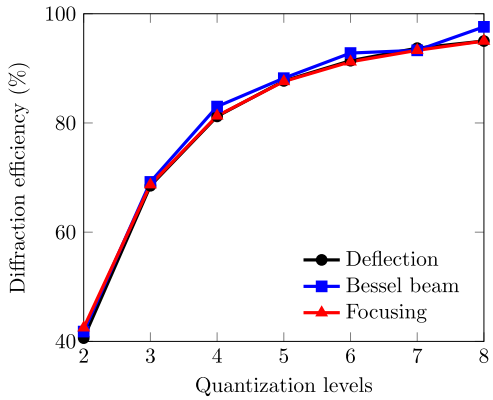

FIG. 6. Investigation of the diffraction efficiency of the three examples of beam control under investigation, namely, beam deflection, Bessel beam generation, and beam focusing.

in free space. By varying the slab thickness as a function of lateral position, this effect can be exploited in order to achieve a given phase distribution and in doing so produce a desired beam-control operation.

Aside from propagation through a dielectric material, it is also possible to manipulate phase by means of a shaped reflector, which is typically composed of a conducting material. The relative depth of different points of the reflector prescribes the phase acquired as the incident wave travels to the reflector and as the reflected wave travels away. In this way, the topology of the reflector may be tailored to achieve a variety of beam control techniques.

A. Traditional implementation

Perhaps the most widespread example of a path-length beam control device is a convex dielectric lens. This is capable of focusing, as the convex curves that define its shape are closely related to the phase characteristic described in Eq. (7). Note that the operation of a lens is most commonly understood in terms of refraction, i.e., the curvature of the dielectric produces the bespoke focusing operation in accordance with Snell's law and ray-tracing optics. That said, both ray-tracing and phase delay paradigms of analysis will show the same focusing behavior for the convex lens. A lens made from a non-dispersive material has extremely high bandwidth, which is advantageous for many applications. This is because the path-length delay given in Eq. (9) scales with frequency in the same way that Eq. (7) does.

Traditional lenses operating in the terahertz range have been commercially available for several years.[79] They are made of materials such as polymers, which offer efficiency in the order of 80%–90%, as well as silicon and quartz, with efficiency of 50%–70%. The origins of loss in devices of this kind are linked to reflection at the dielectric-air boundary, as well as dissipation loss as the beam propagates through the material, as its thickness is non-negligible. This form of loss is common to traditional lenses across the electromagnetic spectrum, but as stated in Sec. I, power is scarce in the terahertz range. Thus, whilst loss of up to 50% may be tolerable in other frequency ranges, it exacerbates fundamental challenges in the terahertz range. Polymer terahertz lenses are also detailed in the literature, having been fabricated with techniques including compression molding and machining.[80–82] These devices operate over a broad bandwidth due to the non-dispersive nature of the polymers employed. Focal lengths from 7 to 60 mm were demonstrated, and the thickness of these devices was up to 15 mm, which is quite large compared to a terahertz wavelength. It is noted that some polymers are visible in both the terahertz and visible ranges. This allows coaxial configurations comprising both optical and terahertz waves.[83] Additional to the dielectrics previously mentioned, there are a few examples of slightly more exotic materials being used for this purpose, including natural stone,[84] as shown in Fig. 7(a), which was 4.1 mm thick, and focused to a distance of ~95 mm over a frequency range from 0.2 to 0.7 THz. Another example is mold-set caramel.[85] However, this device had a limited bandwidth of 0.15–0.4 THz due to the absorptivity of caramel at

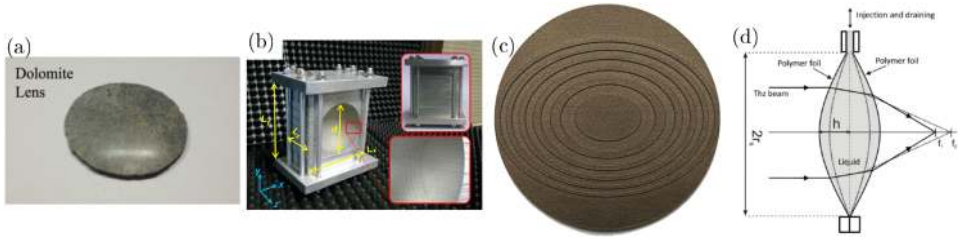

FIG. 7. Various path-length terahertz focusing devices, (a) a convex lens composed of natural stone, after Han *et al.*[84] and (b) a concave lens composed of an all-metal artificial dielectric, with the same functionality as a convex lens, after reprinted with permission from Torres *et al.*, IEEE Trans. Antennas Propag. **63**, 231 (2015). Copyright 2015 IEEE.[93] (c) A reflective stepped-phase device, after Headland *et al.*,[96] and (d) a lens composed of terahertz-transparent liquid enclosed by a polymer bag, where the radius of curvature, and hence the focal length, can be varied by altering the quantity of liquid, after Scherger, Jörgens, and Koch.[97]

higher frequencies. This planoconvex lens had a focal length of approximately 18 mm and was 5 mm thick.

Aside from focusing devices, terahertz-range Bessel beams have been generated using 3D-printed dielectric axicon lenses, with a device thickness of 6.2 mm.[86] Polymer spiral phase plates that are 2 mm-thick have also been employed to realize terahertz vortex beams.[87] These demonstrations illustrate that path-length optics are not limited solely to beam focusing.

B. Artificial dielectrics

Aside from bulk dielectrics, it is also possible to contrive artificial, effective media using periodic, subwavelength structures. From the perspective of an electromagnetic wave, such a structure is experienced as a homogeneous material with properties that are dependent on the structure and potentially different from those of the constituent materials.[88,89] For instance, an array of subwavelength air-holes in a given dielectric material will produce an effective medium that an electromagnetic wave experiences as an artificial dielectric, with an effective refractive index that lies between that of the bulk dielectric and air. This index depends on the hole radius and hole density, and hence it can be controlled by varying the size of the holes with respect to position.

An effective-medium-based device that is analogous to a traditional lens has been constructed from intrinsic silicon, where the effective index (as opposed to device thickness) varied with position in order to achieve the required output phase-front.[90] This device, known as a gradient-index (GRIN) lens, had the advantage of a large bandwidth that is comparable to that of traditional lenses, namely, 0.4–1.6 THz, combined with the extremely thin profile of 100 μm. Additionally, its reduced refractive index resulted in better matching to free-space and hence in greater efficiency. A related device has also been fabricated using 3D printing.[91]

Both of the above artificial dielectrics are constructed entirely from bulk dielectric materials, but other options are available; perhaps counter-intuitively, all-metal structures can also be employed to realize artificial dielectrics. Such a lens is defined from a 2D array of short waveguide sections. Those waveguide sections operate close to the waveguide's cutoff frequency, where fast waves can be observed. Owing to this fast-wave nature, the effective refractive index of the medium is lower than unity. This means that the phase front is accelerated with respect to free space, rather than delayed, as in a conventional medium. Thus, the curvature of lenses of this type is concave, where a traditional lens of the same functionality is convex. Such effective media have been utilized for terahertz lenses,[92–95] as shown in Fig. 7(b). A consequence of employing fast-wave modes is limited bandwidth due to the dispersive nature of non-TEM modes.

C. Wrapped phase

Although the curve-oriented devices in Sec. V A have exceptional bandwidth, they also tend to be quite bulky, and this can limit their aperture and performance. Such devices are therefore most often found in optics laboratory environments. If, on the other hand, compactness is of higher priority than

bandwidth, a stepped- and wrapped-phase arrangement may be preferable. For such a device, first an operating frequency is selected. Subsequently, a suitable level of phase quantization is selected, and this is translated to an appropriate physical step size. This makes stepped-phase devices with phase wrapping more compact than optics based on geometric curves. However, coarse quantization can lead to poor performance, as detailed in Sec. IV B. Furthermore, the phase wrapping procedure is only valid for a single frequency, and hence the overall beam pattern too becomes erroneous as frequency deviates from the operating frequency, in a process known as spatial dispersion. These effects reduce overall device bandwidth, and hence the use of stepped-phase devices represents a trade-off between compactness, aperture, performance, and bandwidth.

Transmissive, stepped-phase diffractive optics have been demonstrated in the terahertz range. Silicon is a highly suitable dielectric material for this purpose, as intrinsic silicon can have very low dissipation, and mature etching techniques are well-suited to produce a quasi-planar device with a finite number of levels.[98–100] These devices were significantly thinner than traditional lenses; the latter cited work had a device thickness of less than 500 μm. In another work, the negative shape of a stepped-lens structure was etched into silicon, and this was used in a stamp-like manner to imprint a stepped-phase focusing structure into a commonly used terahertz transparent polymer known as polypropylene.[101] This material has lower refractive index than silicon and hence exhibits better matching to free-space at the cost of increased physical thickness. This resulted in a device that was 3 mm thick. Another approach to realize stepped polymer devices is compression molding, which has been employed for a terahertz-range blazed diffraction grating that is 4.8 mm-thick.[102] A slightly more unusual choice of dielectric material is ordinary cartridge paper, which was stacked to the requisite thickness for a binary phase difference with respect to free-space, which is ∼1.3 mm, and then the zones of lower-delay were defined by laser-cutting. This resulted in a binary-phase zone plate,[103] and the use of cartridge paper, in particular, represents a highly inventive, low-cost demonstration of a terahertz beam-shaping device. A reflective terahertz zone plate has also been demonstrated, in the form of a 3D-printed metal zone plate, with a focal length of 50 mm.[96] This was fabricated by selective laser melting, and an image of the finished product is given in Fig. 7(c). High-pressure molding presents another means to realize a reflective metal device with a topology that is tailored for operation as a terahertz-range diffraction grating.[104]

D. Reconfigurable optics

Terahertz beam-control devices based on path-length mechanisms can also be made dynamically reconfigurable, and a few examples of such techniques are discussed in this section. Perhaps the most straightforward example is a mechanically actuated flat mirror, which can be employed as a trivial beam-scanning mechanism. There are numerous examples in the literature of terahertz scanning systems of this type.[105–107] However, the need for motorized control, as well as the physical scale of devices of this type, pose serious disadvantages. A more compact, flat-profile approach to mechanically actuated terahertz beam scanning has been demonstrated, which made use of a one-dimensional array of electronically switched reflective cantilevers.[108] Each cantilever could switch between two positions that were separated by a vertical distance of 80 μm, which is an appropriate scale for binary phase difference upon reflection in the terahertz range. This device can therefore achieve dynamic, binary-phase beam scanning, as well as variable focusing in a single dimension in a manner similar to a cylindrical lens. A scanning range of 42° was demonstrated at an operating frequency of 0.33 THz. Although the binary phase is a drawback for reasons discussed in Sec. IV B, the electronic control and compactness of the device are certainly great advantages.

Previously given examples of switchable path-length optics were reflective devices exclusively, but the dynamic control of path-length is also possible for transmissive devices. For instance, one demonstration of a variable-focus lens has made use of a liquid terahertz-transparent dielectric material rather than a solid.[97] In order to maintain a lens-like shape, this liquid was piped into a volume enclosed by a polymer film, and the curvature was dependent on the amount of fluid enclosed. Thus, the focal length of a device of this type can be varied by injection and draining of fluid, as illustrated in Fig. 7(d). In another example from the same group, solid-state control was employed for a wedge-shaped beam-scanning device.[109] The refractive index of this device was varied by applying

a bias voltage to a liquid crystal. For a liquid crystal, the DC electric field aligns the molecules of the birefringent material, and this alters its refractive index. In this way, the output directionality was switchable between two beams separated by a modest ∼ 6°.

VI. PHASED ARRAYS

From an antenna theory perspective, the most prominent and well-known technique associated with beam steering, beamforming, or beam manipulation in general is the phased array antenna. Such a device is essentially a direct, practical realization of the array theory paradigm introduced in Sec. II B; each element in an array of identical, individually excited antennas possesses their own particular amplitude and phase, and the overall pattern of excitation dictates the behavior of the radiated beam.[77] If the phase is controlled with actively tunable phase shifters, the radiation pattern can be dynamically scanned. A schematic of a classical phased array antenna is given in Fig. 8. Key components are the source, which generates the signal to be radiated, a feed network, which makes use of power splitters and bend structures to distribute this signal, controllable phase shifters, and an array of radiating antennas.

In a key example of phased array operation, the phase distribution given in Eq. (4) is employed to achieve beam steering, which in this case equates to a progressive phase difference, $\Delta\varphi$, between adjacent elements,

$$\varphi_n = \varphi_{n-1} + \Delta\varphi. \tag{10}$$

The relationship between the progressive phase, $\Delta\varphi$, and the output steering angle, θ_s, is trivially derived from Eq. (4), by substituting $\Delta\varphi$ for $\varphi(d)$,

$$\Delta\varphi = -k_0 d \sin\theta_s, \tag{11}$$

where it is noted that the spacing between antenna elements, d, must be lower than a free-space wavelength. Failure to observe this condition will result in the existence of grating lobes, which are so-called because they are the product of diffraction effects, and hence their directionality is dictated by the grating equation given in Eq. (5). It is considered as good practice to space the elements at most a half-wave apart. Beam steering of this type is certainly one of the more popular and well-known applications for phased arrays, but as mentioned in Sec. III, shaped-beam techniques are also available, and they provide significant freedom for defining an arbitrary radiation pattern.

A phased array antenna of this kind is chiefly dependent on an efficient feed network, in order to separate the power from a single source into several individual feeds. If, on the other hand,

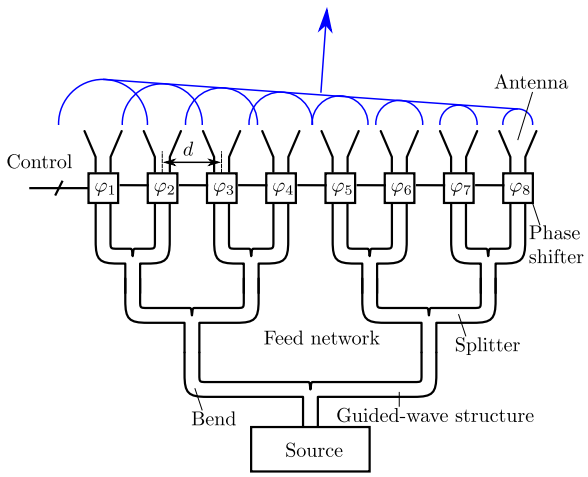

FIG. 8. Schematic illustration of a traditional phased array antenna. Power is generated by the source and distributed to the antenna array by means of a feed network. Prior to radiation, an array of discrete phase shifters is employed to prescribe the required phase distribution for the desired beam shape.

multiple independent sources were to be used, they would not be coherently phased (i.e., their relative phase is not explicitly known or controllable), which makes phased array operation impossible. One notable exception includes separate oscillators that are electronically coupled, but there are practical limitations surrounding the number of elements that can be combined in this way. The performance of a feed network is dependent on the existence of efficient wave-guiding structures. Such components are available at radio and microwave frequencies in the form of microstrip transmission lines and hollow metallic waveguides,[110] as metals are good conductors at these frequencies, and mature fabrication techniques exist. Similarly, in the optical range, advances in nanophotonics have resulted in numerous examples of dielectric waveguides.[111–114] In the terahertz range, however, there are limitations to the efficiency of available wave-guiding structures. This is partly due to the fact that conductivity and skin-depth both decrease as frequency increases.[14,115,116] Thus, metals that operate as good conductors at lower frequencies typically make for inefficient terahertz-range transmission-lines and waveguides. That said, high-resistivity silicon-based dielectric waveguides, similar to the sort that is popular in the optical range, are showing promise in the terahertz range.[117,118] However, it should be noted that the larger wavelength of terahertz radiation compromises the compactness of such structures, and hence this presents a trade-off.

Of equal importance to the feed network is the electronically controllable phase shifter. Such components are mature in the microwave range and have been demonstrated in the millimeter range several decades ago.[119] The majority of such devices rely on varactors to alter the distributed capacitance of a transmission line section, which has not yet been demonstrated in the terahertz range. This is because even advanced CMOS varactors are typically limited by their series resistance to frequencies below 100 GHz.[120] In the optical range, approaches such as thermo-optical tuning[121] and electro-optic modulators[122] are generally preferred for active phase control. To date there has been no demonstration of an electronically controlled phase modulator in the terahertz range that is amenable to integration with a phased array of this type. Another consideration for phase shifters is bandwidth, which can be improved with true time delay techniques that produce a nondispersive phase shift across a given spectral band.[123] This feature is important to maintain a beam pattern that is consistent for a range of frequencies.

Although the components that are integral to classical phased array antennas have not yet been developed in the terahertz range, frequency-conversion presents an alternative means to realize phased arrays. In such a methodology, the feed network and phase shifters operate in a different frequency range, such as the optical or millimeter-wave range. Energy is then converted to the terahertz range at the point of radiation, with phase that is dictated by the pre-conversion signal.

A. Optical feed network

Phased-array-like antennas based on photonics principles have previously been demonstrated in the terahertz range. For instance, one example replaced the need for a terahertz-range feed network with an equivalent network composed of optical fibers, which carried infrared light.[124] These fibers terminated in nonlinear devices, in which optical power was converted to terahertz power by difference frequency generation. This is a well-established method of generating terahertz radiation based on the photomixing of two infrared laser beams of differing colors, where the difference between the two frequencies lies in the terahertz range.[125,126] Controlling the delay in the optical fibers results in a corresponding relative delay of terahertz pulses, which is sufficient for dynamic beam control. This principle was employed to generate a terahertz-range focal spot at a dynamically adjustable position, but the demonstrated scanning range was quite low. A related approach is illustrated in Fig. 9(a), where the photomixer device is fed from free-space rather than optical fibers, and one of the incident infrared beams is tilted to produce a phase gradient.[127,128] In difference-frequency generation, variation in the phase of one of the pump beams will produce an identical variation in the output phase of the terahertz radiation.[129] As such, the aforementioned phase gradient is imparted to the outgoing terahertz beam, resulting in beam steering. Equation (4) shows that the steering angle is relative to wavelength, and hence a given phase gradient will result in a far larger steering angle in the terahertz range than in the infrared range. By tilting the pump beam through a modest 0.155°, a 0.6 THz beam was steered through 29°. The cited work also gives experimental results spanning

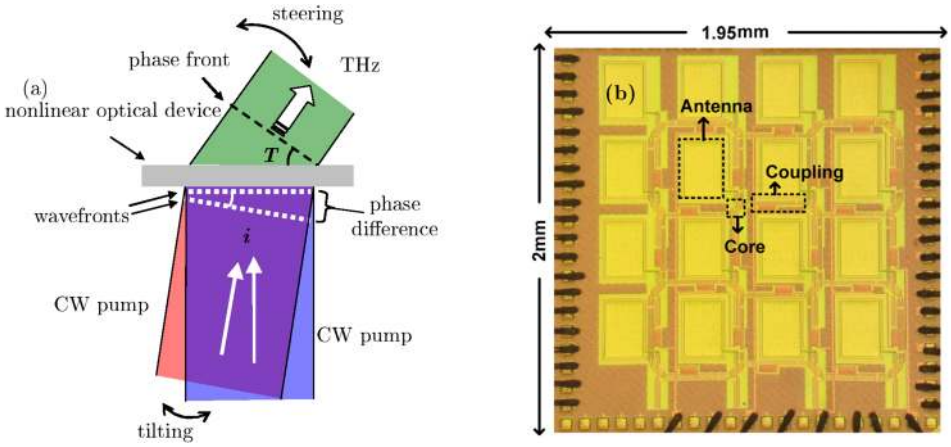

FIG. 9. Terahertz beam-scanning phased array devices, showing (a) an illustration of difference-frequency generation, in which one of the input pump beams was tilted, which translated to a linear phase ramp characteristic in the output beam, after Maki *et al.*[127] and (b) a micrograph of a terahertz phased array antenna with 4×4 elements, based on electronic frequency multipliers, after reprinted with permission from Y. Tousi and E. Afshari, IEEE J. Solid-State Circuits **50**, 597 (2015). Copyright 2015 IEEE.

from 0.3 to 1.7 THz, which illustrates the capacity for this technique to span a broad portion of the terahertz range. This is certainly an encouraging demonstration, but the fact that it requires a sophisticated dual-laser apparatus with mechanical actuation places stringent limitations on feasible practical applications and alignment.

Aside from difference-frequency generation, it is also possible to convert optical power to terahertz radiation using a photoconductive antenna. For such a device, an optical pulse generates free carriers in a semiconductor material, and these carriers are subsequently accelerated toward electrodes by an applied DC electric field. The acceleration of charges in this way generates a broadband terahertz-range pulse.[130] By inverting the polarity of this bias field, it is possible to introduce a π phase shift, or negation, to the radiated terahertz field, and this principle has been employed to realize a binary-phased diffraction grating.[131] A sinusoidal pattern of bias voltage was applied to a dense array of photoconductive antennas, resulting in periodic, binary-phased alternation in the outgoing terahertz field distribution. The spatial period of this sinusoid is defined the symmetrical outgoing beam direction, as per Eq. (5). With this technique, the outgoing terahertz-range beam was steered over 40° at 480 GHz. However, the fact that this device is limited to binary phase poses a disadvantage.

B. Millimeter-wave feed network

Aside from photomixing-oriented techniques, a more practical approach to realize a phased array antenna in the terahertz range is to employ an array of local electronic terahertz sources, based on complimentary metal-oxide-semiconductor (CMOS) technology, which are coupled directly to their adjacent radiators. As the terahertz power generation occurs at the radiator itself, this once again avoids the need for a lossy terahertz feed network. However, the key challenge to address for phased array operation is the synchronization of the different sources such that they are of well-defined relative phase, as is necessary for beam control. In one example, a millimeter-wave frequency reference oscillator was distributed via a feed network to several frequency-multiplier-chain terahertz sources.[132] In the process of feeding, the frequency of the reference signal was split into quadrature signals, which could be added with particular weights at the terahertz source in order to achieve specific values of output phase. This is a clear demonstration of a dynamic-scanning phased array architecture operating in the terahertz range. In this work, a 4×4-element array was fabricated, demonstrating +9.4 dBm effective isotropic radiated power (EIRP) at 280 GHz, with an impressive 2D scanning range of over 80°. However, there are limits to the scalability of a millimeter-wave feed network,

albeit less stringent than in the terahertz range. A more scalable approach to a frequency multiplier-oriented terahertz phased array is to de-centralize the millimeter-wave feed network by coupling individual nodes to their neighbors rather than to a single millimeter-wave source.[133] Varactor-based phase shifters were employed in order to produce a relative phase shift between adjacent nodes, and this phase shift in the millimeter-wave signal translated to a corresponding phase shift in the radiated terahertz signal. Although the demonstrated device was of the same number of elements as in the previously discussed work (i.e., 4×4), it is more promising for the development of larger arrays. Furthermore, the array exhibited higher output power, namely, +17.1 dBm EIRP at 338 GHz, with a scanning range of 45° in one dimension and 50° in the other. An image of the fabricated CMOS chip is given in Fig. 9(b). Another approach to synchronization is to mutually couple neighboring terahertz sources via near-field effects, which has been demonstrated at 200 GHz.[134] However, the limitations to array scalability in this case are more restrictive, and hence a 2×2 array was demonstrated. The output power was −1.9 dBm EIRP at 191 GHz, and the 2D scanning range was 70°.

VII. LEAKY-WAVE ANTENNAS

Leaky-wave antennas (LWAs) can perform beamforming and beam steering by coherently leaking a traveling wave from a waveguide into free-space. The traveling wave acquires phase as it propagates through its guiding structure, and in the simplest form, this translates to a linear phase ramp of the sort discussed in Sec. III B, upon gradual radiation to free-space. A LWA device can be considered as being equivalent to phased arrays, where the crucial distinction is that LWAs operate in series, whereas phased arrays radiate from multiple points in parallel. In the microwave range, LWAs have been used for several decades,[135] and they have a similarly long history in the optical regime, where they are known as grating couplers.[136] The application of LWAs to terahertz frequencies has recently been emerging due to the prospect of directional beamforming with a low-profile aperture. This feature is particularly relevant in the terahertz regime due to the limitations upon the efficiency and complexity of phased-array antennas discussed in Sec. VI. Furthermore, the compatibility of LWAs with active sources[137,138] and electronically reconfigurable materials[139,140] is promising for integrated terahertz systems. One salient feature of LWAs is that the output beam direction is dependent upon frequency. This limits the bandwidth that a leaky-wave antenna can project into a single direction, but it can also be viewed as a feature, as it is a means to achieve dynamic scanning simply by sweeping frequency. That said, the ability to make use of this feature is chiefly dependent upon the existence and performance of compatible tunable sources. In the terahertz range, such sources are typically limited in terms of their speed of tuning, tuning range, and efficiency.[141,142] Additionally, the loss that is typical of terahertz-range transmission lines and waveguides negatively impacts the achievable aperture of LWAs, as the distance that a guided wave can travel is reduced.

Regardless of the frequency range, LWAs are classified into two categories: either a slow-wave or fast-wave.[64] The slow-wave type is constructed with a waveguide in which the phase velocity is slower than the speed of light. Slow waves take place in, for example, dielectric-loaded TEM transmission lines and dielectric waveguides. The guided wave does not leak into free-space spontaneously due to the phase or momentum mismatch, and hence it requires periodic scatterers or a grating for free-space coupling. As such, slow-wave LWAs are also known as periodic LWAs. A slow-wave LWA with periodic scatterers is illustrated in Fig. 10(a). The output beam angle is described by the following phase-matching condition:

$$k_0 \sin\theta_s = \beta + \frac{2\pi m}{p}, \quad m = 0, \pm 1, \pm 2, \ldots, \tag{12}$$

where k_0 is the free-space wavenumber, β is the guided-wave propagation constant, which is larger than k_0, p is the grating periodicity, which is around a wavelength of the guided mode, and θ_s is the beam angle measured from broadside. This reconciles with Eq. (4) when the equation is multiplied by p, as it becomes clear that the difference in phase between a radiator at $x = 0$ and $x = p$ is determined by the product of the propagation constant and distance, $p\beta$, plus any number of complete phase

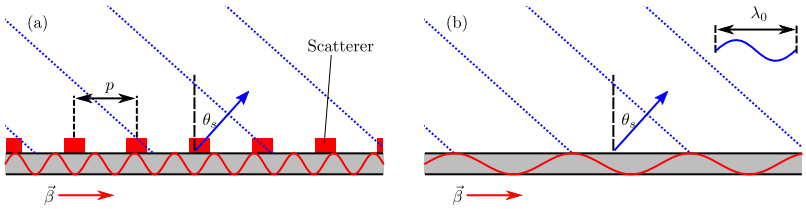

FIG. 10. Illustration of (a) a slow-wave leaky-wave antenna, for which $\beta = 2k_0$. and (b) a fast-wave antenna, for which $\beta = \frac{2}{3}k_0$. Scatterers are incorporated into the slow-wave structure as it is nonradiative, but these are not necessary for the fast-wave structure.

cycles, $2\pi m$. Single-order diffraction is achieved when β is designed so that a real-valued θ_s exists only for $m = -1$. The beam angle, θ_s, can be directed from backward ($\theta_s < 0$) to forward ($\theta_s > 0$) across broadside ($\theta_s = 0$) when k_0 and β are varied by sweeping the frequency.

On the other hand, for a fast-wave LWA, the phase velocity exceeds the speed of light, leading to $\beta < k_0$. This faster phase velocity means that the apparent wavelength inside the waveguide becomes longer than in free-space. In this case, a real-valued θ_s can exist even in the absence of a grating, as the traveling wave spontaneously leaks into free-space. As such, Eq. (12) takes the following form:

$$k_0 \sin\theta_s = \beta. \tag{13}$$

Such antennas are also known as uniform LWAs, as opposed to periodic LWAs. This is illustrated in Fig. 10(b). In the case of a rectangular waveguide, the two media in and outside the waveguide must be connected, for example, through a slot. The continuous aperture can suppress sidelobes and higher-order diffraction. Note that, in this case, Eq. (12) becomes equivalent to Snell's Law with the grazing incident angle. A fast-wave LWA mechanism is achieved with non-TEM modes in waveguides[143] and in composite right/left handed (CRLH) transmission lines.[144,145] Most fast-wave LWAs can launch only forward beams ($\theta_s > 0$) as the sign of β is fixed positive. However, CRLH transmission lines can support either forward or backward beams, as they possess a band with negative phase velocity, or backward waves, with $\beta < 0$.

In LWAs, the guided waves experience desirable radiation losses and undesirable material losses during propagation, resulting in a non-uniform amplitude profile along the radiation aperture. To optimize the beam pattern, this spatial amplitude decay can be compensated by increasing the radiation efficiency along the aperture.[64] A possible extension to LWAs is spatial control of the phase profile. While LWAs are mostly intended for directional beamforming with constant θ_s, i.e., for beam deflection as detailed in Sec. III B, spatially modulating β and p such that θ_s varies spatially can emulate diffractive optics.[146] Based on this concept, more specialized beams such as focused beams[147] and Bessel beams[148] can be generated, which is particularly relevant in the terahertz regime to replace bulky optical components. Such a concept can further be generalized under the waveguide-hologram developed in optics,[149] although the design is basically valid for a single frequency as inferred from Eq. (12).

A. Slow-wave implementations

Most slow-wave structures, including transmission lines and dielectric waveguides, are amenable to planar fabrication techniques, which can readily accommodate features with sizes of ten microns. These guiding structures are thus attractive for terahertz applications. One demonstration under this category is based on a microstrip line that supports a quasi-TEM mode. In this work, a LWA was implemented around 300 GHz by patterning copper on low-loss cyclo-olefin polymer (COP),[43] as shown in Fig. 11(a). Periodic stubs incorporated on the microstrip line can convert the guided mode into a TE-polarized directional beam. As the transverse electric field along the microstrip line is mirror-symmetric, those staggered stubs on both sides can double the array density to enhance the radiation efficiency, suppress grating lobes, and widen the aperture in the transverse direction. It is noted that the presence of the periodic stubs modifies the propagation constant and attenuation

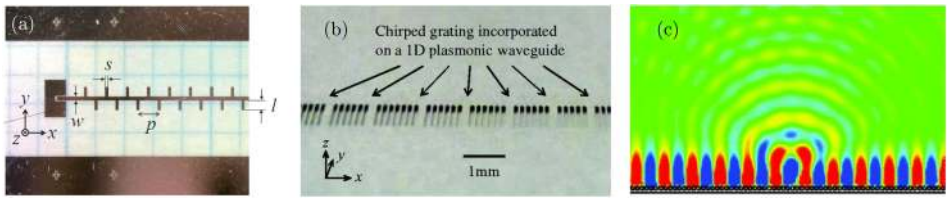

FIG. 11. Implementations of LWAs in the terahertz range, showing (a) a transmission line with interdigitated stub scatterers operating around 300 GHz, after reprinted with permission from Murano *et al.*, IEEE Trans. Terahertz Sci. Tech. **7**, 60 (2017). Copyright 2017 IEEE. (b) A plasmonic LWA, which omits specific grooves in a chirped arrangement so as to achieve terahertz-range focusing and (c) an illustration of plasmonic wave confinement, with scattering from a single omitted groove, after reprinted with permission from Monnai *et al.*, Appl. Phys. Lett. **101**, 151116 (2012). Copyright 2012 AIP Publishing LLC.

coefficient of the unloaded microstrip line. Accounting for these effects is important in order to predict the beam angle and width precisely. Another design consideration for periodic LWAs is an open stop band at broadside, where $\beta p = 2\pi$. In this case, broadside radiation is significantly suppressed due to the Bragg reflection of the guided mode.[150–152] For this particular work, optimization of the stub geometry can mitigate or negate the stop band. In an experimental demonstration, a directional beam was steered from −23° to +15° across broadside by sweeping the frequency from 235 to 325 GHz. The authors also demonstrated its application in terahertz radar.

Surface waves are considered to be another type of slow waves, which propagate along a boundary of different media with an evanescent field away from the surface. As the field confinement of surface-waves is relatively loose, they are easily launched into free-space by incorporating weak perturbation onto the surface. Structures supporting surface waves can be made of either a dielectric slab or a subwavelength-corrugated metal. It is noted that the latter sustains surface-waves in the form of spoof surface plasmon polaritons,[153,154] which are not scattered by the subwavelength-scale corrugation. While the use of dielectric slabs is advantageous to reduce transmission losses, the use of corrugated metals offers greater dispersion control. An example of a terahertz LWA defined on a corrugated metal surface was implemented with aperiodic modulation of the groove depth.[147] The resulting contrast of the surface impedance serves as a scatterer that launches the guided mode into free-space. The spacing between adjacent scatterers was chirped, which yielded beam-focusing toward a point at 30 mm above the surface at 300 GHz. A portion of this device is shown in Fig. 11(b), and the launched wave due to a single scatterer is shown in Fig. 11(c). The chirped structure is designed so that scattered waves interfere constructively at a single point in free-space, and explicit formulas that dictate the scatterer arrangement are available.[155]

Another example of a slow-wave terahertz LWA has been demonstrated with a dielectric waveguide.[156] The waveguide, together with a chirped dielectric grating, was fabricated by means of 3D printing of polystyrene. A prototype printed with a 0.1 mm layer resolution has demonstrated diffraction-limited focusing at 120 GHz. Notably, although the scatterers were loaded on one face of the waveguide, power was observed to project to both upper and lower halves of the space. Such dielectric LWAs require a metal reflector at its back to launch waves only into the upper-half space.

The lateral aperture size of LWAs implemented from 1D guiding structures is strictly limited, and this results in beam broadening in this dimension. However, structures sustaining surface waves can be expanded into 2D. So-called bullseye structures made of concentric subwavelength metal grooves can be regarded as such an example. By means of radially periodic scatterers, radially spreading surface waves excited through a central slit are converted into azimuthally distributed plane waves in free-space. The use of a 2D aperture also allows access to beam families that cannot be generated with a 1D LWA. One such example is a Bessel beam, which is detailed in Sec. III C. According to Eq. (12), a grating with a period p slightly shorter than the wavelength of a guided mode leads to $\theta_s < 0$, i.e., beam tilting toward the central axis. A TM_1 Bessel beam is then formed as a result of the interference of those tilted plane waves.[148] The beam width changes very little over a propagation distance of more than 35 mm—nearly 35λ at 290 GHz.

B. Fast-wave implementations

Fast-wave LWAs, which do not require periodic scatterers, have been commonly used in the microwave range in the form of a rectangular waveguide incorporating a continuous radiating slot along one of the side walls.[64] Although the same mechanism is valid in the terahertz range, the fabrication of such non-planar structures becomes very demanding at micro-scale. As an alternative, the use of a parallel-plate waveguide in the TE_1 mode has been demonstrated.[143] The TE_1 mode is the lowest order transverse electric mode with a modal index less than one, or equivalently, $\beta < k_0$.[157] A radiating slot is incorporated on the top metal plate along the propagation direction. The beam angle can be varied from +5° to +80° by sweeping the frequency from 150 to 500 GHz.[143] Although the TE_1 guided waves are likely to diffract in plane, it can be negated by a gradient or curved plate separation in the transversal direction. Later, a similar leaky-wave antenna has been employed for terahertz communications.[158] In this case, spatial dispersion of the beam allows frequency-multiplexing inside the waveguide. In that demonstration, each individual channel bore data rates of 10 Gbps, with an aggregate data rate of 50 Gbps. For non-TEM modes in parallel-plate waveguides, the plate separation governs the propagation constant, β. Thus, LWAs can exploit this dependence to vary the beam angle in accordance with Eq. (13). By smoothly varying the separation of the two plates along the propagation axis, beam-focusing can be achieved. A prototype of a focusing LWA has been constructed by combining a slotted flat aluminum plate with a curved bottom surface fabricated via 3D printing.[159] Focusing above the top plate has been experimentally demonstrated at 100 GHz and 170 GHz.

As mentioned earlier, CRLH transmission lines can sustain leaky fast waves with positive and negative propagation constants. Such a CRLH transmission line was implemented at terahertz frequencies to observe mode behaviors.[145] In addition, another similar CRLH transmission line was co-fabricated with a terahertz source—a quantum cascade laser.[137] The authors demonstrated discrete beam steering in the forward direction within a range of 25° when the frequency is tuned from 2.65 to 2.81 THz. The authors added that backward scanning is possible by including series capacitance along the line to access the regime of negative phase velocity.[137]

A 2D implementation for fast-wave LWAs exists in the form of Fabry–Pérot cavity resonator antennas.[160] In this case, the LWA was defined by a planar gap between a ground plane and the base of a hemispherical lens made of silicon and was fed by a slot-terminated rectangular waveguide attached to the ground plane. This leaky-wave structure on its own did not perform beamforming directly but was used as a directive primary feed for the lens. The leaky radiation helps to expand the aperture of the rectangular waveguide. An experimental demonstration confirmed beam collimation with high directivity at 545 GHz.

VIII. REFLECTARRAYS AND TRANSMITARRAYS

Reflectarray and transmitarray antennas (henceforth "passive arrays" when considered collectively) consist of a 2D array of nonuniform, subwavelength elements that interact with free-space fields. When a single element of the array is excited by incident radiation, it will impart some particular local phase shift upon the re-radiated wave. Ideally, this phase shift can be any value in a 360° cycle and is wholly independent of the phase shift that is imparted by neighboring elements. Taken collectively, these local phase shifts produce some overall desired phase distribution, which is associated with a bespoke output beam pattern. Given the flat profile of the device, and the mutual independence of the phase shift imparted by different elements, there is a significant amount of design freedom in the device's functionality.

If the outgoing waves are radiated from the same face that accepts the incident radiation (i.e., they are reflected), then the device is a reflectarray. On the other hand, if the outgoing waves are radiated from the opposite face, then the device is a transmitarray. There are advantages and trade-offs in each case; a transmitarray is generally more susceptible to losses and may require either polarization converters or multi-layer configurations[161] in order to achieve the required phase tunability range. On the other hand, a reflectarray has added complications due to feed blockage, where the feed antenna is in the path of the far-field beam. Thus, the choice of reflectarray or transmitarray is dependent on

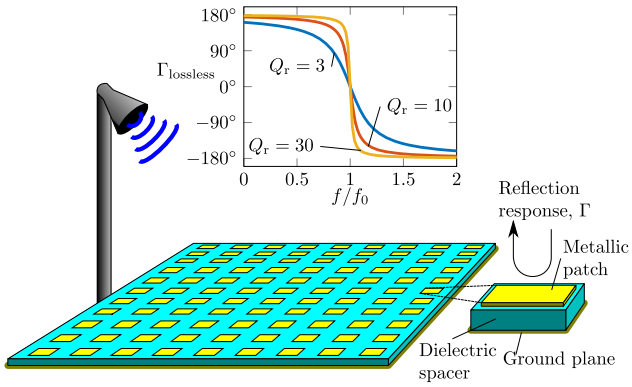

FIG. 12. Diagram of a reflectarray antenna, with a simple horn-antenna feed. In this case, the unit cell resonator is a metallic patch that is separated from a metallic ground plane by a dielectric spacer. In this idealized case, both the metal and dielectric are lossless, so reflection is expressed in terms of phase response exclusively, as magnitude response is unity in all cases.

the particular requirements of the specific application at hand. A diagram of a reflectarray antenna, showing resonator elements and feed structure, is given in Fig. 12.

Passive arrays can be considered as a combination of phased array antennas and geometric optics. Outgoing waves with a tailored phase distribution emerge from a planar array, similar to the phased array discussed in Sec. VI. However, the feed is via free space, much like geometric optics in Sec. V. This approach has the advantage over traditional phased array antennas of not requiring a feed network, as well as supporting far greater overall antenna apertures. Furthermore, passive arrays have the advantage of being far more compact than geometric optics, and even more so than stepped optics, as their phase is acquired instantaneously. However, a caveat is that passive arrays typically exhibit spatial dispersion due to the dispersive response of resonators, as well as the necessity of phase wrapping, and hence they do not enjoy the same high bandwidth of geometric optics. Lastly, passive arrays generally offer high efficiency and the potential for birefringence (i.e., independent control of different polarizations), which are both highly beneficial properties.

Very often, passive array devices of this sort are termed "nonuniform metasurfaces" or more specifically, "flat optics," especially in the terahertz and optical ranges.[162–164] This represents a convergence between different fields of study and is entirely valid. Metasurfaces have grown out of the paradigm of metamaterials, in which a volumetric array of periodic inclusions results in an effective medium with controllable and at times exotic properties that depend on the geometry and constituent bulk materials of these inclusions.[165] A metasurface is simply a planar or quasi-planar version of a metamaterial, a single quasi-2D portion of a metamaterial's volume.[166,167] As such, there is no substantive difference between a passive array and a nonuniform metasurface designed for beam control, aside from a tendency for the latter to make use of more deeply subwavelength cells. In this article, however, the terminology of "reflectarrays" and "transmitarrays" is adopted, as the initial demonstration of reflectarray antennas precedes the advent of metamaterials by several decades.[168]

The phase discontinuity that a passive array depends upon is generally realized using passive resonators to establish electric and/or magnetic dipoles. The following is a discussion that focuses on reflective resonators, for reflectarray antenna devices such as that which is illustrated in Fig. 12, but similar principles of operation apply to transmissive devices. An infinite array of identical, subwavelength, reflective resonators that interacts with incident free-space fields can be modeled as a one-port network with complex reflection coefficient Γ. The following expression for the reflection coefficient of a resonator is employed to explore the connection between passive resonators and phase control:[169]

$$\Gamma = \frac{Q_a}{\frac{Q_a}{2} + \frac{Q_r}{2} + jQ_rQ_a\left(\frac{f}{f_0} - 1\right)} - 1. \tag{14}$$

This models a resonator with a single mode of resonance, which is described by the resonance frequency f_0, the radiation quality factor Q_r, and the absorption quality factor Q_a. The latter two quantities relate to energy exchanged with free space and energy lost to dissipation, respectively. For the resonators best-suited to beam control devices, the condition $Q_a \gg Q_r$ is assumed, which describes efficient resonators with strong free-space coupling. An ideal case of this, in which no energy is dissipated, corresponds to $Q_a \to \infty$. Under this condition, the reflection coefficient reduces to the following form:

$$\Gamma_{\text{lossless}} = \frac{\frac{1}{2} - jQ_r\left(\frac{f}{f_0} - 1\right)}{\frac{1}{2} + jQ_r\left(\frac{f}{f_0} - 1\right)}. \tag{15}$$

The magnitude of this expression is always equal to 1, as no power is dissipated in the one-port network. On resonance (i.e., $f = f_0$), the response is purely real, and the phase of the reflected wave is 0°. It is noted that this condition alone defines an artificial magnetic conductor (AMC), as opposed to a perfect electric conductor (PEC) with a reflection phase response of −180°. Away from resonance, however, the phase response deviates progressively from 0° and in cases of high Q_r, heads to +180° as $f \to 0$ and −180° as $f \to \infty$, respectively. Thus, if the frequency of operation, f, is gradually detuned from the resonance frequency, f_0, the resonator can cover a range of reflection phase close to 360°. This form of phase control as a consequence of frequency-tuning is shown in the plot in Fig. 12. The operation of a given reflectarray antenna is therefore dependent on the capacity to tune the resonance frequency, f_0, of a passive resonator away from the operating frequency, f. In all examples presented in this review, this is achieved by means of adjusting the physical geometry of the resonator in question. It can be seen from the plot in Fig. 12 that, in general, a higher value of Q_r engenders a larger phase tunability range. However, higher Q_r also leads to a more rapid phase transition, and this is intrinsically more sensitive to phase errors associated with fabrication tolerances.

A. Reflectarrays

1. Metallic resonators

Terahertz-range reflectarray antennas have previously been reported. In the first such demonstration, an array of square, micro-scale metallic patches was deposited onto a uniform-thickness polydimethylsiloxane (PDMS) slab, which rested on a platinum-coated silicon substrate.[170] These grounded patches support a cavity resonance that is equivalent to two magnetic dipoles. As such, patches of this sort are resonant structures and are covered by Eq. (14), where the resonance frequency is determined by patch dimensions. Thus, a nonuniform layout of patches can be employed to impart a specific required phase distribution onto reflected beams. In the referenced work,[170] the required beam-shaping operation is deflection at an operating frequency of 1 THz, and hence it employs a linear ramp, as in Eq. (4). Phase is necessarily wrapped in order to accommodate the finite phase tunability

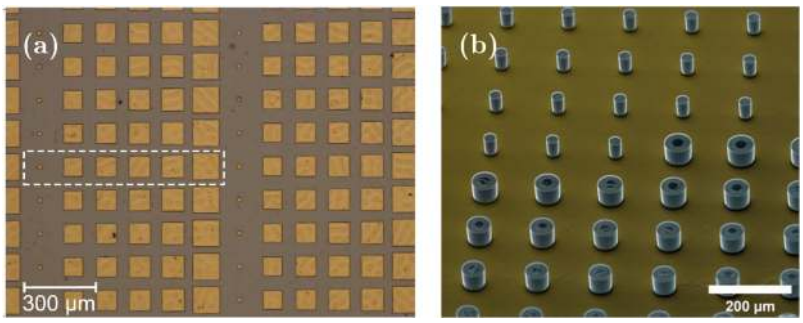

FIG. 13. Two different reflectarray devices for operation at 1 THz, showing (a) a portion of a periodic metallic-resonator reflectarray, with a single period indicated with a white dashed line, after Niu *et al.*[170] and (b) a portion of a DRA-based reflectarray, after reprinted with permission from Headland *et al.*, ACS Photonics **3**, 1019 (2016). Copyright 2016 American Chemical Society.

range of the resonator, and the resulting structure is shown in Fig. 13(a). The required beam-shaping behavior was experimentally verified, but the overall efficiency with which energy was deflected to the desired direction was below 64%. The same author has since expanded on this methodology, employing rectangular patches[55] and striplines,[56] to achieve birefringent deflection, which provides the capacity to process different polarizations separately. However, the peak efficiency reported in each referenced work was below 56% and 40%, respectively. Given that one of the main motivations for terahertz beam control given in Sec. I is to minimize wasted power, it is desirable to have higher overall efficiency. In this case, the majority of loss originates in the PDMS spacer, as it is a moderately lossy dielectric in the terahertz range.[16] Lower-loss polymers such as polypropylene have been employed for metallic resonator-based reflectarrays in the terahertz range, producing reflectarrays with 80% efficiency at 350 GHz.[171] In another demonstration, high-resistivity silicon served as a dielectric spacer for a reflectarray that operated in three bands, namely, 0.7 THz, 1.0 THz, and 1.5 THz, with efficiency of 60%–70%.[172]

2. Dielectric resonators

The above demonstrations, in Sec. VIII A 1, have laid the foundation for reflectarray antennas in the terahertz range. However, a common issue that they share is efficiency that is lower than desirable. One reason for this is that metallic resonators often employ a polymer dielectric spacer, and such materials are generally moderately lossy in the terahertz range. Additionally, metals are not ideal conductors in the terahertz range, as conductivity and skin depth decrease as the frequency is increased,[14,115,116] which engenders Ohmic dissipation that is enhanced by field confinement on-resonance.

Dielectric resonators that are composed of low-loss dielectric materials present an alternative to metallic resonators for use in terahertz reflectarrays. Such resonators operate by means of confinement at the dielectric-air boundary; a wave originating inside a small volume of moderate-to-high index dielectric will be redirected back into the dielectric at this boundary, only to meet another such interface, and so on. This forms a standing wave, which is a mode of resonance of the sort covered by Eq. (14). In this case, resonance is of displacement current rather than conduction current. Thus, a dielectric resonator exhibits lower Ohmic dissipation than a metallic resonator. Additionally, unlike metallic resonators, dielectric resonators do not need to be separated from the ground plane, and hence there is no need for an often-lossy polymer spacer. Taken together, these features make for resonators that are of superior efficiency to those detailed in Sec. VIII A 1.

Arrays of terahertz-range dielectric resonator antennas (DRAs) have previously been presented. The first such demonstration made use of titanium dioxide (TiO_2), which has a relative permittivity of greater than 100, as the low-loss dielectric material.[174] Subsequently, uniform arrays of resonators employing high-resistivity silicon, which has a relative permittivity[175] of $\epsilon \sim 11.68$ in the terahertz range, were demonstrated.[176,177] The more-moderate relative permittivity of the dielectric employed in the latter two cases is better suited to terahertz reflectarray applications, as it engenders a lower Q_r that is more amenable to precise phase control. Additionally, dielectric resonators of this sort have numerous higher-order modes of resonance, which jointly produce a large phase transition. Thus, the lower quality factor does not prevent the dielectric resonator from having a full, geometrically tuned 360° phase range.

The aforementioned dielectric resonators[176] were subsequently adapted into a nonuniform layout to serve as a focusing mirror reflectarray.[173] A micrograph of a portion of the fabricated device is given in Fig. 13(b), showing nonuniform silicon resonators on a gold ground plane. The focusing functionality of this device was verified experimentally, and device loss was determined to be negligible to within experimental error within an 18% bandwidth centered around 1 THz. Thus, this is a compact (i.e., flat-profile) and efficient device that is capable of shaping terahertz radiation. Furthermore, the demonstrated device had over 80 000 elements in total, with a total diameter of over 160 wavelengths, and hence overall aperture was extremely large. However, dielectric resonator antennas are not easily integrable with tunable structures such as varactors, which is a technique that has led to beam-scanning reflectarrays at lower frequencies.[58,178,179] As such, less-efficient metallic resonators yield greater potential for tunability. Additionally, it is challenging to make dielectric resonator antennas of this sort birefringent, as this engenders a large number of asymmetric modes that

are highly sensitive to the nonuniformity of reflectarrays. This tends to produce spurious reflection phase and polarization impurity in DRA-based birefringent reflectarrays. Thus, there is a trade-off; metallic resonators offer greater versatility than DRAs in reflectarray devices, but due to the Ohmic loss of metals in the terahertz range, their efficiency is lower than desirable.

B. Transmitarrays

Reports of terahertz-range transmitarrays are far more common than reflectarrays in the literature. Most often, terahertz-range transmitarrays operate in cross-polarization. For such a device, the energy that is commuted into the same polarization as the incident beam (co-polarization) is minimized, and the orthogonal (cross-polarization) is maximized. Typically, the unit cell of such a transmitarray is an anisotropic, metallic resonator. The mode of resonance consists of current vectors with components that are parallel to both the co- and cross-polarized electric field directions. Currents that are excited by the co-polarized incident field will therefore radiate in the cross-polarization. For this reason, complementary "V"[180–183] and "C"-shaped[44,184] metallic resonators, such as that which is shown in Fig. 14(a), are a popular choice, as these shapes are naturally amenable to this form of commutation of current vectors. In general, this technique provides a higher degree of phase tunability than is achievable when utilizing transmitted co-polarization. This is because mirroring a given resonator will essentially produce a π phase shift in transmitted cross-polarized radiation, as the orientation of the current vectors that give rise to this outgoing wave is reversed.

Devices employing "V"-shaped resonators sort offer conversion to cross-polarization with modest efficiency up to ~25% and have been demonstrated for terahertz flat lenses, frequency-scanning beam steerers, and vortex beams. The operation bandwidth of the "V"-shaped resonators is typically in the order of ~30%, and the "C"-shaped resonators can achieve 60%, but it is worth noting that this does not translate directly to practical device bandwidth due to the spatial dispersion characteristics of flat optics.

A related approach makes use of a multi-layer structure, for which the first and third layers are essentially orthogonal wire-grid polarizers, and the middle layer bears the resonators. The polarizer layers block co-polarized transmission through the device, as well as cross-polarized reflection from the resonator layer, and this improves the conversion to cross-polarized transmission. This has been employed for a beam-deflector device, which achieved a peak efficiency of 60%–80%, with a broad usable bandwidth from 0.5 to 1.8 THz.[185] Subsequently, this methodology was employed to realize a flat lens device with a center frequency of 400 GHz and overall focusing efficiency of 68%.[186] A micrograph of a portion of this array is given in Fig. 14(b). Both devices represent a significant improvement upon previously demonstrated polarization-converting terahertz transmitarrays.

For transmitarrays that shape the co-polarization rather than the cross-polarization, multiple layers of resonators are needed to achieve the required phase tunability range.[161,187] At lower frequencies, this option is preferable, as the necessity of polarization conversion is undesirable, and also precludes any possibility of birefringent control. However, metals do not behave as ideal conductors

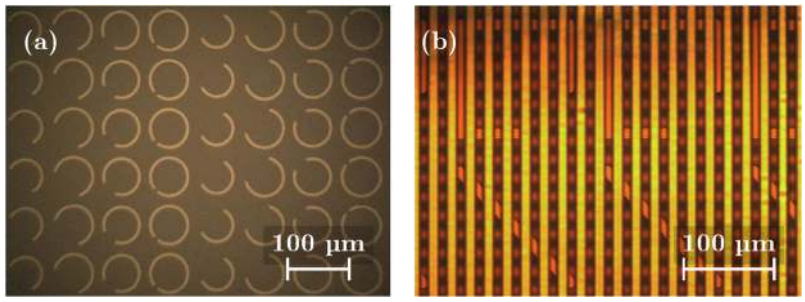

FIG. 14. Terahertz-range transmitarrays that operate in cross-polarization, showing (a) a micrograph of a nonuniform array of C-shaped resonators, which is a portion of a transmitarray device, after Zhang *et al.*,[44] and (b) a multi-layer metallic transmitarray, where the top and bottom layers are orthogonal wire-grid polarizers that enhance the yield of cross-polarized radiation, after Chang *et al.*[186]

at terahertz frequencies,[14] and hence the addition of more resonator layers engenders an increase in Ohmic loss. For example, a three-layer device consisting of "I"-shaped resonator unit cells has been employed for a frequency-scanning beam steerer operating around 0.9 THz, with a peak efficiency of 44%.[188] Another example of a three-layer device performs focusing, in which the individual resonator element is a complementary metallic annulus, and the phase response is tuned by its radius.[189] One drawback of employing complementary structures of this type is that the transmittance is only acceptable close to the resonance frequency, and hence by detuning the resonance frequency away from the operating frequency in order to manipulate phase response, the efficiency is severely impacted. For instance, at the operating frequency of 1.3 THz, the peak efficiency of the resonator was ~68%, but when the center-frequency of the resonator's passband is closer to 1.6 THz, the efficiency at 1.3 THz dropped to 1.7%. Subsequent work by the same author employed a single resonator layer, resulting in efficiency above 35% at the operating frequency of 1.3 THz, and this was deployed for a beam steering device.[190] However, the use of a single layer has the pronounced disadvantage of a reduced phase tunability range, and this is evidenced in the modest deflection angle of 6° at 1.3 THz.

IX. COMPARISON

This section contrasts the benefits and disadvantages of the various terahertz-range beam control techniques that are presented in this article. A summary of the key findings of this comparison is provided in Table I.

From the above analysis of published studies in the field of terahertz-range beam control, a few considerations become immediately apparent. First, the bandwidth offered by traditional lenses, such as those presented in Sec. V, is unparalleled by any other beam-shaping technique. However, the physical bulk of such devices poses a drawback. Stepped-phase devices sacrifice bandwidth for a quasi-flat profile, but such devices typically remain several wavelengths thick. Additionally, most reported stepped-phase devices are transmissive, and hence there is a trade-off between the reflection loss and device thickness that is mediated by the selection of refractive index. Additionally, it is difficult to generate complicated and reconfigurable beam profiles using path-length optics.

With regards to phased arrays, the low-loss feed networks and compact phase shifters that they depend upon have yet to be demonstrated in the terahertz range. Thus, *in lieu* of a classical terahertz phased array, terahertz-range devices have so-far made use of frequency conversion. Although the photonic beam control mechanisms discussed in Sec. VI are impressive demonstrations, they require highly specialized laser equipment that is unlikely to be amenable to practical, consumer-oriented

TABLE I. A comparison of the four beamforming techniques that are presented in this article, in terms of important performance criteria for operation in the terahertz range. Numerical values of performance are provided in instances in which they are applicable, but it is noted that only approximate estimates are possible, given the breadth of devices covered. Furthermore, due to their differences in operating principles and beam-control operations, a direct comparison of performance is not always possible. Thus, this comparison should only be taken as a guide.

Technique	Path-length	Phased array	LWA	Passive array
Complexity	Low	High	Moderate	Moderate
Radiation efficiency	Moderate for transmissive (typically 40%–80%), high for reflective (close to 100%)	Low (numerical value unclear due to frequency-conversion)	Moderate (~80%)	High (up to ~100% for dielectric resonators, ~70% for metallic resonators)
Bandwidth	High (no phase wrapping; >100%)	Low (5%–20%)	Moderate (<10% for fixed direction and >100% frequency-scanning)	Low (10%, spatial-dispersion limited)
Aperture	High (F-number typically >1, limited by bulkiness)	Low (<4λ width)	Moderate (20–30λ in one dimension)	Very high (>100λ in diameter)
Compactness	Low (significant thickness and separation from feed)	High	High	Moderate (requires separation from feed)
Tunability	Strictly limited	Dynamic scanning	Frequency-scanning	Potential
Versatility	Low	High	Moderate	High
Feed type	Free-space	Point feed	Point feed	Free-space

applications. The electronic beam-control devices presented in the same section are encouraging, but there are limitations in achievable physical scale and operating frequency, and hence it is not clear whether such devices will provide a complete solution to the problem of terahertz-range beam control.

The leaky-wave antennas discussed in Sec. VII can integrate a large, albeit generally-1D aperture antenna with a source and detector—all in a planar profile. Since it is viewed as a series-fed antenna array, beam steering is achieved by sweeping the frequency. However, this can also pose a drawback, as the bandwidth that can be projected into a single beam direction is limited. Similar to phased arrays, decreasing material losses in the waveguide is a current technical challenge.

The reflectarrays and transmitarrays presented in Sec. VIII are compact, large-aperture, and of a high degree of versatility in terms of the beam-shaping operation that they perform. Thus, they address many of the limitations posed by the above beam-shaping techniques. However, the majority of the passive arrays presented exhibited efficiency that is insufficient for adoption into practical technologies. Advances in terahertz dielectric resonator antennas have led to highly efficient terahertz reflectarrays,[173] as detailed in Sec. VIII A 2. However, there are also disadvantages in this work; the bandwidth of the resultant structure was limited by spatial dispersion, and the beam-shaping operation that the device performed was static. Additionally, passive arrays cannot easily be directly integrated with sources and detectors, and hence the overall compactness of systems that make use of such devices is diminished by the need for a free-space feed.

X. CONCLUSION

This article reconciles knowledge and techniques for beamforming across the microwave and photonics domains, which have historically been separated by nature. The article focuses on state-of-the-art terahertz beam control, which benefits from both domains. It is asserted that the unique applications of terahertz waves engender a necessity for beamforming. The basic underlying principle of wavefront engineering, which is essentially the correspondence between aperture phase distribution and output beam behavior, is presented abstractly. Significant demonstrations that have made use of these principles are presented, and these demonstrations fell under the following categories: traditional optics, phased array antennas, leaky-wave antennas, and passive arrays. These approaches are compared and contrasted.

Our aim is to provide the required context for future investigations into terahertz beam control. In order to expedite progress toward practical applications, research efforts should be concentrated in a few areas. First, dynamic, electronically controlled beam scanning using solid-state electronic devices are required for several prospective applications. Phased array antennas have demonstrated such a capacity, albeit with constraints on efficiency, aperture, and complexity. Reconfigurable path-length devices have been demonstrated, but the tuning mechanism is either mechanical in nature or stringently limited. Second, bandwidth enhancement is another focus, particularly to benefit terahertz communications. Aside from geometric optics, which possess large bandwidth, stepped optics, leaky-wave antennas, reflectarrays, and transmitarrays alike experience what is known as spatial dispersion; their beam shape varies with respect to frequency, and this limits the achievable bandwidth of a single link. In the case of reflectarrays and phased array antennas, this can be partially addressed with true-time delay techniques,[191] but this has not yet been demonstrated in the terahertz range. Lastly, efficiency is a major hurdle in many beamforming structures. By addressing this challenge, precious terahertz power can be preserved to enhance performance in sensing, imaging, and communications.

ACKNOWLEDGMENTS

We acknowledge support from the Australian Research Council Discovery Project (No. ARC DP170101922).

[1] H. Rubens and E. Nichols, Phys. Rev. **4**, 314 (1897).
[2] J. Chamberlain, Philos. Trans. R. Soc., A **362**, 199 (2004).
[3] E. Nichols and J. Tear, Astrophys. J. **61**, 17 (1925).
[4] P. H. Siegel, IEEE Trans. Microwave Theory Tech. **50**, 910 (2002).

[5] U. R. Pfeiffer, Y. Zhao, J. Grzyb, R. Al Hadi, N. Sarmah, W. Förster, H. Rücker, and B. Heinemann, IEEE J. Solid-State Circuits **49**, 2938 (2014).
[6] P. Hillger, J. Grzyb, S. Malz, B. Heinemann, and U. Pfeiffer, in *Radio Frequency Integrated Circuits Symposium* (IEEE, 2017), pp. 160–163.
[7] M. Asada, S. Suzuki, and N. Kishimoto, Jpn. J. Appl. Phys., Part I **47**, 4375 (2008).
[8] T. Maekawa, H. Kanaya, S. Suzuki, and M. Asada, Appl. Phys. Express **9**, 024101 (2016).
[9] J. H. Booske, R. J. Dobbs, C. D. Joye, C. L. Kory, G. R. Neil, G.-S. Park, J. Park, and R. J. Temkin, IEEE Trans. Terahertz Sci. Technol. **1**, 54 (2011).
[10] W. He, L. Zhang, D. Bowes, H. Yin, K. Ronald, A. Phelps, and A. Cross, Appl. Phys. Lett. **107**, 133501 (2015).
[11] T. Nagatsuma, G. Ducournau, and C. C. Renaud, Nat. Photonics **10**, 371 (2016).
[12] S. Lepeshov, A. Gorodetsky, A. Krasnok, E. Rafailov, and P. Belov, Laser Photonics Rev. **11**, 1600199 (2017).
[13] ITU-R, "676-10 Attenuation by Atmospheric Gases," 2013.
[14] P. Drude, Ann. Phys. **306**, 566 (1900).
[15] P. D. Cunningham, N. N. Valdes, F. A. Vallejo, L. M. Hayden, B. Polishak, X.-H. Zhou, J. Luo, A. K.-Y. Jen, J. C. Williams, and R. J. Twieg, J. Appl. Phys. **109**, 043505 (2011).
[16] I. Khodasevych, C. Shah, S. Sriram, M. Bhaskaran, W. Withayachumnankul, B. Ung, H. Lin, W. Rowe, D. Abbott, and A. Mitchell, Appl. Phys. Lett. **100**, 061101 (2012).
[17] E. V. Fedulova, M. M. Nazarov, A. A. Angeluts, M. S. Kitai, V. I. Sokolov, and A. P. Shkurinov, Proc. SPIE **8337**, 83370I (2012).
[18] M. Naftaly, *Terahertz Metrology* (Artech House, 2015).
[19] J. A. Zeitler, P. F. Taday, D. A. Newnham, M. Pepper, K. C. Gordon, and T. Rades, J. Pharm. Pharmacol. **59**, 209 (2007).
[20] Y.-C. Shen, Int. J. Pharm. **417**, 48 (2011).
[21] J. F. Federici, B. Schulkin, F. Huang, D. Gary, R. Barat, F. Oliveira, and D. Zimdars, Semicond. Sci. Technol. **20**, S266 (2005).
[22] P. Taday, I. Bradley, D. Arnone, and M. Pepper, J. Pharm. Sci. **92**, 831 (2003).
[23] K. Kawase, Y. Ogawa, Y. Watanabe, and H. Inoue, Opt. Express **11**, 2549 (2003).
[24] W. R. Tribe, D. A. Newnham, P. F. Taday, and M. C. Kemp, Proc. SPIE **5354** (2004).
[25] D. J. Cook, B. K. Decker, G. Maislin, and M. G. Allen, Proc. SPIE **5354** (2004).
[26] W. S. L. Lee, S. Nirantar, D. Headland, M. Bhaskaran, S. Sriram, C. Fumeaux, and W. Withayachumnankul, "Broadband Terahertz Circular-Polarization Beam Splitter," Adv. Opt. Mater. (published online).
[27] M. Yamaguchi, F. Miyamaru, K. Yamamoto, M. Tani, and M. Hangyo, Appl. Phys. Lett. **86**, 053903 (2005).
[28] M. Franz, B. M. Fischer, and M. Walther, J. Mol. Struct. **1006**, 34 (2011).
[29] A. B. True, K. Schroeck, T. A. French, and C. A. Schmuttenmaer, J. Infrared, Millimeter, Terahertz Waves **32**, 691 (2011).
[30] B. Hu and M. Nuss, Opt. Lett. **20**, 1716 (1995).
[31] C. B. Reid, E. Pickwell-MacPherson, J. G. Laufer, A. P. Gibson, J. C. Hebden, and V. P. Wallace, Phys. Med. Biol. **55**, 4825 (2010).
[32] C. Yu, S. Fan, Y. Sun, and E. Pickwell-MacPherson, Quant. Imaging Med. Surg. **2**, 33 (2012).
[33] J. Y. Suen and W. J. Padilla, Appl. Phys. Lett. **108**, 233701 (2016).
[34] A. Luukanen, R. Appleby, M. Kemp, and N. Salmon, *Terahertz Spectroscopy and Imaging* (Springer, 2013), pp. 491–520.
[35] J. B. Jackson, J. Bowen, G. Walker, J. Labaune, G. Mourou, M. Menu, and K. Fukunaga, IEEE Trans. Terahertz Sci. Technol. **1**, 220 (2011).
[36] G. C. Walker, J. W. Bowen, W. Matthews, S. Roychowdhury, J. Labaune, G. Mourou, M. Menu, I. Hodder, and J. B. Jackson, Opt. Express **21**, 8126 (2013).
[37] A. Fitzgerald, E. Berry, N. Zinov'ev, S. Homer-Vanniasinkam, R. Miles, J. Chamberlain, and M. Smith, J. Biol. Phys. **29**, 123 (2003).
[38] J. Bjarnason, T. Chan, A. Lee, M. Celis, and E. Brown, Appl. Phys. Lett. **85**, 519 (2004).
[39] D. M. Mittleman, R. H. Jacobsen, and M. C. Nuss, IEEE J. Sel. Top. Quantum Electron. **2**, 679 (1996).
[40] S. Busch, G. Town, M. Scheller, and M. Koch, J. Infrared, Millimeter, Terahertz Waves **36**, 318 (2015).
[41] R. Jain, J. Grzyb, and U. R. Pfeiffer, IEEE Trans. Terahertz Sci. Technol. **6**, 649 (2016).
[42] J. Grajal, A. Badolato, G. Rubio-Cidre, L. Úbeda-Medina, B. Mencia-Oliva, A. Garcia-Pino, B. Gonzalez-Valdes, and O. Rubiños, IEEE Trans. Microwave Theory Tech. **63**, 1097 (2015).
[43] K. Murano, I. Watanabe, A. Kasamatsu, S. Suzuki, M. Asada, W. Withayachumnankul, T. Tanaka, and Y. Monnai, IEEE Trans. Terahertz Sci. Technol. **7**, 60 (2017).
[44] X. Zhang, Z. Tian, W. Yue, J. Gu, S. Zhang, J. Han, and W. Zhang, Adv. Mater. **25**, 4567 (2013).
[45] C. E. Shannon, Bell Syst. Tech. J. **27**, 379 (1948).
[46] C. E. Shannon, Proc. IRE **37**, 10 (1949).
[47] H.-J. Song, K. Ajito, Y. Muramoto, A. Wakatsuki, T. Nagatsuma, and N. Kukutsu, Electron. Lett. **48**, 953 (2012).
[48] K. Ishigaki, M. Shiraishi, S. Suzuki, M. Asada, N. Nishiyama, and S. Arai, Electron. Lett. **48**, 582 (2012).
[49] S. Koenig, D. Lopez-Diaz, J. Antes, F. Boes, R. Henneberger, A. Leuther, A. Tessmann, R. Schmogrow, D. Hillerkuss, R. Palmer, T. Zwick, C. Koos, W. Freude, O. Ambacher, J. Leuthold, and I. Kallfass, Nat. Photonics **7**, 977 (2013).
[50] H.-J. Song, J.-Y. Kim, K. Ajito, N. Kukutsu, and M. Yaita, IEEE Trans. Microwave Theory Tech. **62**, 600 (2014).
[51] S. Kitagawa, S. Suzuki, and M. Asada, Electron. Lett. **52**, 479 (2016).
[52] X. Yu, S. Jia, H. Hu, M. Galili, T. Morioka, P. U. Jepsen, and L. K. Oxenløwe, APL Photonics **1**, 081301 (2016).
[53] S. Diebold, K. Nishio, Y. Nishida, J.-Y. Kim, K. Tsuruda, T. Mukai, M. Fujita, and T. Nagatsuma, Electron. Lett. **52**, 1999 (2016).
[54] D. Headland, T. Niu, E. Carrasco, D. Abbott, S. Sriram, M. Bhaskaran, C. Fumeaux, and W. Withayachumnankul, IEEE J. Sel. Top. Quantum Electron. **23**, 8500918 (2017).

[55] T. Niu, W. Withayachumnankul, A. Upadhyay, P. Gutruf, D. Abbott, M. Bhaskaran, S. Sriram, and C. Fumeaux, Opt. Express **22**, 16148 (2014).
[56] T. Niu, A. Upadhyay, W. Withayachumnankul, D. Headland, D. Abbott, M. Bhaskaran, S. Sriram, and C. Fumeaux, Appl. Phys. Lett. **107**, 031111 (2015).
[57] B. Desiatov, N. Mazurski, Y. Fainman, and U. Levy, Opt. Express **23**, 22611 (2015).
[58] S. V. Hum, M. Okoniewski, and R. J. Davies, IEEE Microwave Compon. Lett. **15**, 422 (2005).
[59] M. Riel and J.-J. Laurin, IEEE Trans. Antennas Propag. **55**, 1260 (2007).
[60] E. Hecht, *Optics*, 4th ed. (Addison-Wesley, 2002).
[61] J. W. Goodman, *Introduction to Fourier Optics* (Roberts and Company Publishers, 2005).
[62] S. Schelkunoff, Bell Syst. Tech. J. **15**, 92 (1936).
[63] S. Silver, J. Opt. Soc. Am. **52**, 131 (1962).
[64] J. Volakis, *Antenna Engineering Handbook*, 4th ed. (McGraw-Hill Book Company, 2007).
[65] F. Ahmad, M. G. Amin, and S. A. Kassam, IEEE Trans. Aerosp. Electron. Syst. **41**, 271 (2005).
[66] S. Tokoro, K. Kuroda, A. Kawakubo, K. Fujita, and H. Fujinami, in *Proceedings of IEEE Intelligent Vehicles Symposium, 2003* (IEEE, 2003), pp. 304–309.
[67] J. Durnin, J. Miceli, Jr, and J. Eberly, Phys. Rev. Lett. **58**, 1499 (1987).
[68] S. Monk, J. Arlt, D. Robertson, J. Courtial, and M. Padgett, Opt. Commun. **170**, 213 (1999).
[69] R. Herman and T. Wiggins, J. Opt. Soc. Am. A **8**, 932 (1991).
[70] T. A. Planchon, L. Gao, D. E. Milkie, M. W. Davidson, J. A. Galbraith, C. G. Galbraith, and E. Betzig, Nat. Methods **8**, 417 (2011).
[71] H. Meng, B. Xiang, J. Zhang, W. Dou, and Y. Yu, J. Infrared, Millimeter, Terahertz Waves **35**, 208 (2014).
[72] M. Beijersbergen, R. Coerwinkel, M. Kristensen, and J. Woerdman, Opt. Commun. **112**, 321 (1994).
[73] J. Arlt and M. Padgett, Opt. Lett. **25**, 191 (2000).
[74] R. W. Gerchberg and W. O. Saxton, Optik **35**, 237 (1972).
[75] D.-W. Duan and Y. Rahmat-Samii, IEEE Trans. Antennas Propag. **43**, 27 (1995).
[76] F. J. Villegas, IEEE Trans. Antennas Propag. **55**, 1745 (2007).
[77] C. A. Balanis, *Antenna Theory: Analysis and Design* (John Wiley & Sons, 2016).
[78] B. E. Saleh and M. C. Teich, *Fundamentals of Photonics*, 2nd ed. (Wiley, New York, 2007).
[79] G. Kropotov and E. Tsygankova, *Siberian J. Phys.*, Series: Physics (Vestnik Novosibirsk State Univserity, 2010), Vol. 5.
[80] B. Scherger, M. Scheller, C. Jansen, M. Koch, and K. Wiesauer, Appl. Opt. **50**, 2256 (2011).
[81] M. Wichmann, A. Mondol, N. Kocic, S. Lippert, T. Probst, M. Schwerdtfeger, S. Schumann, T. Hochrein, P. Heidemeyer, M. Bastian, and M. Koch, Appl. Opt. **52**, 4186 (2013).
[82] N. V. Chernomyrdin, M. E. Frolov, S. P. Lebedev, I. V. Reshetov, I. E. Spektor, V. L. Tolstoguzov, V. E. Karasik, A. M. Khorokhorov, K. I. Koshelev, A. O. Schadko, S. O. Yurchenko, and K. I. Zaytsev, Rev. Sci. Instrum. **88**, 014703 (2017).
[83] M. Yamashita, C. Otani, K. Kawase, K. Nikawa, and M. Tonouchi, Appl. Phys. Lett. **93**, 041117 (2008).
[84] D. Han, K. Lee, J. Lim, S. S. Hong, Y. K. Kim, and J. Ahn, Appl. Opt. **52**, 8670 (2013).
[85] L. A. Sterczewski, M. P. Grzelczak, K. Nowak, and E. F. Plinski, Opt. Eng. **55**, 090505 (2016).
[86] X. Wei, C. Liu, L. Niu, Z. Zhang, K. Wang, Z. Yang, and J. Liu, Appl. Opt. **54**, 10641 (2015).
[87] K. Miyamoto, K. Suizu, T. Akiba, and T. Omatsu, Appl. Phys. Lett. **104**, 261104 (2014).
[88] T. C. Choy, *Effective Medium Theory: Principles and Applications* (Oxford University Press, 2015), Vol. 165.
[89] D. Headland, P. Thurgood, D. Stavrevski, W. Withayachumnankul, D. Abbott, M. Bhaskaran, and S. Sriram, Opt. Mater. Express **5**, 1373 (2015).
[90] S.-G. Park, K. Lee, D. Han, J. Ahn, and K.-H. Jeong, Appl. Phys. Lett. **105**, 091101 (2014).
[91] A. Hernandez-Serrano, M. Weidenbach, S. Busch, M. Koch, and E. Castro-Camus, J. Opt. Soc. Am. B **33**, 928 (2016).
[92] M. Navarro-Cía, M. Beruete, I. Campillo, and M. Sorolla, Phys. Rev. B **83**, 115112 (2011).
[93] V. Torres, B. Orazbayev, V. Pacheco-Peña, J. Teniente, M. Beruete, M. Navarro-Cía, M. S. Ayza, and N. Engheta, IEEE Trans. Antennas Propag. **63**, 231 (2015).
[94] R. Mendis, M. Nagai, Y. Wang, N. Karl, and D. M. Mittleman, Sci. Rep. **6**, 23023 (2016).
[95] T. Suzuki, T. Kimura, T. Togashi, H. Kitahara, K. Ishihara, and T. Sato, Appl. Phys. A **123**, 139 (2017).
[96] D. Headland, W. Withayachumnankul, M. Webb, H. Ebendorff-Heidepriem, A. Luiten, and D. Abbott, Opt. Express **24**, 17384 (2016).
[97] B. Scherger, C. Jördens, and M. Koch, Opt. Express **19**, 4528 (2011).
[98] S. Wang, T. Yuan, E. Walsby, R. Blaikie, S. Durbin, D. Cumming, J. Xu, and X.-C. Zhang, Opt. Lett. **27**, 1183 (2002).
[99] S. C. Saha, C. Li, Y. Ma, J. P. Grant, and D. R. Cumming, IEEE Trans. Terahertz Sci. Technol. **3**, 479 (2013).
[100] L. Minkevičius, S. Indrišiūnas, R. Šniaukas, B. Voisiat, V. Janonis, V. Tamošiūnas, I. Kašalynas, G. Račiukaitis, and G. Valušis, Opt. Lett. **42**, 1875 (2017).
[101] E. Walsby, J. Alton, C. Worrall, H. Beere, D. Ritchie, and D. Cumming, Opt. Lett. **32**, 1141 (2007).
[102] B. Scherger, N. Born, C. Jansen, S. Schumann, M. Koch, and K. Wiesauer, IEEE Trans. Terahertz Sci. Technol. **2**, 556 (2012).
[103] A. Siemion, A. Siemion, M. Makowski, J. Suszek, J. Bomba, A. Czerwiński, F. Garet, J.-L. Coutaz, and M. Sypek, Opt. Lett. **37**, 4320 (2012).
[104] S. F. Busch, N. Born, M. Koch, and B. Fischer, J. Infrared, Millimeter, Terahertz Waves **34**, 413 (2013).
[105] K. B. Cooper, R. J. Dengler, N. Llombart, T. Bryllert, G. Chattopadhyay, E. Schlecht, J. Gill, C. Lee, A. Skalare, I. Mehdi, and P. H. Siegel, IEEE Trans. Microwave Theory Tech. **56**, 2771 (2008).
[106] K. B. Cooper, R. J. Dengler, N. Llombart, B. Thomas, G. Chattopadhyay, and P. H. Siegel, IEEE Trans. Terahertz Sci. Technol. **1**, 169 (2011).
[107] A. B. Kos and E. Gerecht, J. Res. Natl. Inst. Stand. Technol. **118**, 125 (2013).

[108] Y. Monnai, K. Altmann, C. Jansen, H. Hillmer, M. Koch, and H. Shinoda, Opt. Express **21**, 2347 (2013).
[109] B. Scherger, M. Reuter, M. Scheller, K. Altmann, N. Vieweg, R. Dabrowski, J. A. Deibel, and M. Koch, J. Infrared, Millimeter, Terahertz Waves **33**, 1117 (2012).
[110] D. M. Pozar, *Microwave Engineering* (John Wiley & Sons, 2009).
[111] M. Lončar, T. Doll, J. Vučlović, and A. Scherer, J. Lightwave Technol. **18**, 1402 (2000).
[112] S. J. McNab, N. Moll, and Y. A. Vlasov, Opt. Express **11**, 2927 (2003).
[113] Y. Jiang, L. Jiang, W. Gu, X. Chen, and R. T. Chen, Appl. Phys. Lett. **87**, 221105 (2005).
[114] X. Liu, R. M. Osgood, Y. A. Vlasov, and W. M. Green, Nat. Photonics **4**, 557 (2010).
[115] M. K. Kazimierczuk, *High-Frequency Magnetic Components* (John Wiley & Sons, 2009).
[116] L. Zou, W. Withayachumnankul, C. Shah, A. Mitchell, M. Klemm, M. Bhaskaran, S. Sriram, and C. Fumeaux, IEEE Photonics J. **6**, 4600110 (2014).
[117] K. Tsuruda, M. Fujita, and T. Nagatsuma, Opt. Express **23**, 31977 (2015).
[118] M. Yata, M. Fujita, and T. Nagatsuma, Opt. Express **24**, 7835 (2016).
[119] H. Jacobs and M. M. Chrepta, IEEE Trans. Microwave Theory Tech. **22**, 411 (1974).
[120] T. Quemerais, D. Gloria, D. Golanski, and S. Bouvot, IEEE Electron Device Lett. **36**, 87 (2015).
[121] J. Sun, E. Timurdogan, A. Yaacobi, E. S. Hosseini, and M. R. Watts, Nature **493**, 195 (2013).
[122] J. Nees, S. Williamson, and G. Mourou, Appl. Phys. Lett. **54**, 1962 (1989).
[123] I. Frigyes and A. Seeds, IEEE Trans. Microwave Theory Tech. **43**, 2378 (1995).
[124] S. Bauerschmidt, G. Döhler, H. Lu, A. Gossard, S. Malzer, and S. Preu, Opt. Lett. **38**, 3673 (2013).
[125] S. Matsuura, M. Tani, and K. Sakai, Appl. Phys. Lett. **70**, 559 (1997).
[126] M. Tani, P. Gu, M. Hyodo, K. Sakai, and T. Hidaka, Opt. Quantum Electron. **32**, 503 (2000).
[127] K.-I. Maki and C. Otani, Opt. Express **16**, 10158 (2008).
[128] K.-I. Maki, T. Shibuya, C. Otani, K. Suizu, and K. Kawase, Appl. Phys. Express **2**, 022301 (2009).
[129] A. M. Sinyukov, Z. Liu, Y. L. Hor, K. Su, R. B. Barat, D. E. Gary, Z.-H. Michalopoulou, I. Zorych, J. F. Federici, and D. Zimdars, Opt. Lett. **33**, 1593 (2008).
[130] M. Van Exter, C. Fattinger, and D. Grischkowsky, Appl. Phys. Lett. **55**, 337 (1989).
[131] N. M. Froberg, B. B. Hu, X. C. Zhang, and D. H. Auston, IEEE J. Quantum Electron. **28**, 2291 (1992).
[132] K. Sengupta and A. Hajimiri, IEEE J. Solid-State Circuits **47**, 3013 (2012).
[133] Y. Tousi and E. Afshari, IEEE J. Solid-State Circuits **50**, 597 (2015).
[134] K. Sengupta and A. Hajimiri, IEEE Trans. Microwave Theory Tech. **63**, 2867 (2015).
[135] F. K. Schwering and S. T. Peng, IEEE Trans. Microwave Theory Tech. **31**, 199 (1983).
[136] A. Yariv and M. Nakamura, IEEE J. Quantum Electron. **13**, 233 (1977).
[137] A. A. Tavallaee, B. S. Williams, P. W. Hon, T. Itoh, and Q.-S. Chen, Appl. Phys. Lett. **99**, 141115 (2011).
[138] N. Yu, Q. J. Wang, M. A. Kats, J. A. Fan, S. P. Khanna, L. Li, A. G. Davies, E. H. Linfield, and F. Capasso, Nat. Mater. **9**, 730 (2010).
[139] M. Esquius-Morote, J. S. Gómez-Diaz, and J. Perruisseau-Carrier, IEEE Trans. Terahertz Sci. Technol. **4**, 116 (2014).
[140] X.-C. Wang, W.-S. Zhao, J. Hu, and W.-Y. Yin, IEEE Trans. Nanotechnol. **14**, 62 (2015).
[141] S. Kitagawa, S. Suzuki, and M. Asada, J. Infrared, Millimeter, Terahertz Waves **35**, 445 (2014).
[142] S. Kitagawa, S. Suzuki, and M. Asada, IEEE Electron Device Lett. **35**, 1215 (2014).
[143] N. J. Karl, R. W. McKinney, Y. Monnai, R. Mendis, and D. M. Mittleman, Nat. Photonics **9**, 717 (2015).
[144] D. R. Jackson, C. Caloz, and T. Itoh, Proc. IEEE **100**, 2194 (2012).
[145] P. W. Hon, Z. Liu, T. Itoh, and B. S. Williams, J. Appl. Phys. **113**, 033105 (2013).
[146] A. Katzir, A. Livanos, J. Shellan, and A. Yariv, IEEE J. Quantum Electron. **13**, 296 (1977).
[147] Y. Monnai, K. Altmann, C. Jansen, M. Koch, H. Hillmer, and H. Shinoda, Appl. Phys. Lett. **101**, 151116 (2012).
[148] Y. Monnai, D. Jahn, W. Withayachumnankul, M. Koch, and H. Shinoda, Appl. Phys. Lett. **106**, 021101 (2015).
[149] T. Suhara and H. Nishihara, IEEE J. Quantum Electron. **22**, 845 (1986).
[150] S. Paulotto, P. Baccarelli, F. Frezza, and D. R. Jackson, IEEE Trans. Antennas Propag. **57**, 1894 (2009).
[151] S. Otto, A. Rennings, K. Solbach, and C. Caloz, IEEE Trans. Antennas Propag. **59**, 3695 (2011).
[152] J. T. Williams, P. Baccarelli, S. Paulotto, and D. R. Jackson, IEEE Trans. Antennas Propag. **61**, 4484 (2013).
[153] F. Garcia-Vidal, L. Martin-Moreno, and J. Pendry, J. Opt. A **7**, S97 (2005).
[154] C. R. Williams, S. R. Andrews, S. Maier, A. Fernandez-Dominguez, L. Martín-Moreno, and F. Garcia-Vidal, Nat. Photonics **2**, 175 (2008).
[155] Y. Monnai and H. Shinoda, IEEE Trans. Antennas Propag. **59**, 2070 (2011).
[156] D. Jahn, M. Weidenbach, J. Lehr, L. Becker, F. Beltrán-Mejía, S. F. Busch, J. C. Balzer, and M. Koch, J. Infrared, Millimeter, Terahertz Waves **38**, 708 (2017).
[157] R. Mendis and D. M. Mittleman, IEEE Trans. Microwave Theory Tech. **58**, 1993 (2010).
[158] J. Ma, N. J. Karl, S. Bretin, G. Ducournau, and D. M. Mittleman, Nat. Commun. **8**, 729 (2017).
[159] R. W. McKinney, Y. Monnai, R. Mendis, and D. Mittleman, Opt. Express **23**, 27947 (2015).
[160] N. Llombart, G. Chattopadhyay, A. Skalare, and I. Mehdi, IEEE Trans. Antennas Propag. **59**, 2160 (2011).
[161] F. Monticone, N. M. Estakhri, and A. Alù, Phys. Rev. Lett. **110**, 203903 (2013).
[162] S.-W. Qu, H. Yi, B. J. Chen, K. B. Ng, and C. H. Chan, Proc. IEEE **105**, 1166 (2017).
[163] N. M. Estakhri and A. Alù, J. Opt. Soc. Am. B **33**, A21 (2016).
[164] A. Epstein and G. V. Eleftheriades, J. Opt. Soc. Am. B **33**, A31 (2016).
[165] D. R. Smith, W. J. Padilla, D. Vier, S. C. Nemat-Nasser, and S. Schultz, Phys. Rev. Lett. **84**, 4184 (2000).
[166] C. L. Holloway, E. F. Kuester, J. A. Gordon, J. O'Hara, J. Booth, and D. R. Smith, IEEE Antennas Propag. Mag. **54**, 10 (2012).
[167] I. Al-Naib and W. Withayachumnankul, J. Infrared, Millimeter, Terahertz Waves **38**, 1067 (2017).
[168] D. Berry, R. Malech, and W. Kennedy, IEEE Trans. Antennas Propag. **11**, 645 (1963).

[169] C. Qu, S. Ma, J. Hao, M. Qiu, X. Li, S. Xiao, Z. Miao, N. Dai, Q. He, S. Sun, and L. Zhou, Phys. Rev. Lett. **115**, 235503 (2015).
[170] T. Niu, W. Withayachumnankul, B. S.-Y. Ung, H. Menekse, M. Bhaskaran, S. Sriram, and C. Fumeaux, Opt. Express **21**, 2875 (2013).
[171] S. A. Kuznetsov, M. A. Astafev, M. Beruete, and M. Navarro-Cía, Sci. Rep. **5**, 7738 (2015).
[172] H. Hasani, M. Tamagnone, S. Capdevila, C. F. Moldovan, P. Maoddi, A. M. Ionescu, C. Peixeiro, J. R. Mosig, A. K. Skrivervik, and J. Perruisseau-Carrier, IEEE Trans. Terahertz Sci. Technol. **6**, 268 (2016).
[173] D. Headland, E. Carrasco, S. Nirantar, W. Withayachumnankul, P. Gutruf, J. Schwarz, D. Abbott, M. Bhaskaran, S. Sriram, J. Perruisseau-Carrier, and C. Fumeaux, ACS Photonics **3**, 1019 (2016).
[174] K. Takano, Y. Yakiyama, K. Shibuya, K. Izumi, H. Miyazaki, Y. Jimba, F. Miyamaru, H. Kitahara, and M. Hangyo, IEEE Trans. Terahertz Sci. Technol. **3**, 812 (2013).
[175] J. Dai, J. Zhang, W. Zhang, and D. Grischkowsky, J. Opt. Soc. Am. B **21**, 1379 (2004).
[176] D. Headland, S. Nirantar, W. Withayachumnankul, P. Gutruf, D. Abbott, M. Bhaskaran, C. Fumeaux, and S. Sriram, Adv. Mater. **27**, 7137 (2015).
[177] Z. Ma, S. M. Hanham, P. Albella, B. Ng, H. T. Lu, Y. Gong, S. A. Maier, and M. Hong, ACS Photonics **3**, 1010 (2016).
[178] S. V. Hum, M. Okoniewski, and R. J. Davies, IEEE Trans. Antennas Propag. **55**, 2200 (2007).
[179] F. Venneri, S. Costanzo, and G. Di Massa, Electron. Lett. **48**, 68 (2012).
[180] D. Hu, X. Wang, S. Feng, J. Ye, W. Sun, Q. Kan, P. J. Klar, and Y. Zhang, Adv. Opt. Mater. **1**, 186 (2013).
[181] X.-Y. Jiang, J.-S. Ye, J.-W. He, X.-K. Wang, D. Hu, S.-F. Feng, Q. Kan, and Y. Zhang, Opt. Express **21**, 30030 (2013).
[182] J. He, X. Wang, D. Hu, J. Ye, S. Feng, Q. Kan, and Y. Zhang, Opt. Express **21**, 20230 (2013).
[183] D. Hu, G. Moreno, X. Wang, J. He, A. Chahadih, Z. Xie, B. Wang, T. Akalin, and Y. Zhang, Opt. Commun. **322**, 164 (2014).
[184] Q. Wang, X. Zhang, Y. Xu, Z. Tian, J. Gu, W. Yue, S. Zhang, J. Han, and W. Zhang, Adv. Opt. Mater. **3**, 779 (2015).
[185] N. K. Grady, J. E. Heyes, D. R. Chowdhury, Y. Zeng, M. T. Reiten, A. K. Azad, A. J. Taylor, D. A. Dalvit, and H.-T. Chen, Science **340**, 1304 (2013).
[186] C.-C. Chang, D. Headland, D. Abbott, W. Withayachumnankul, and H.-T. Chen, Opt. Lett. **42**, 1867 (2017).
[187] Q. Yang, J. Gu, Y. Xu, X. Zhang, Y. Li, C. Ouyang, Z. Tian, J. Han, and W. Zhang, Adv. Opt. Mater. **5**, 1601084 (2017).
[188] S. Liu, Q. Cheng, Q. Xu, T. Q. Wang, L. L. Du, K. Luan, Y. H. Xu, D. Bao, X. J. Fu, J. G. Han, W. L. Zhang, and T. J. Cui, Adv. Opt. Mater. **4**, 384 (2016).
[189] J. Neu, B. Krolla, O. Paul, B. Reinhard, R. Beigang, and M. Rahm, Opt. Express **18**, 27748 (2010).
[190] J. Neu, R. Beigang, and M. Rahm, Appl. Phys. Lett. **103**, 041109 (2013).
[191] E. Carrasco, J. A. Encinar, and M. Barba, IEEE Trans. Antennas Propag. **56**, 2496 (2008).